

## Miocene evolution of the External Rif Zone (Morocco): Comparison with similar and lateral southern Mediterranean Tethyan margins



Manuel Martín-Martín <sup>a,\*</sup>, Francesco Guerrera <sup>b</sup>, Juan Carlos Cañaveras <sup>a</sup>, Francisco Javier Alcalá <sup>c,d</sup>, Francisco Serrano <sup>e</sup>, Alí Maaté <sup>f</sup>, Rachid Hlila <sup>f</sup>, Soufian Maaté <sup>g</sup>, Antonio Sánchez-Navas <sup>h</sup>, Crina Miclăus <sup>i</sup>, José Enrique Tent-Manclús <sup>a</sup>, Manuel Bullejos <sup>j</sup>

<sup>a</sup> Departamento de Ciencias de la Tierra y Medio Ambiente, University of Alicante, AP 99, 03080 Alicante, Spain

<sup>b</sup> Dipartimento di Scienze Pure e Applicate (DiSPeA), Università degli Studi di Urbino Carlo Bo, Campus Scientifico E. Mattei, 61029 Urbino, Italy

<sup>c</sup> Departamento de Desertificación y Geo-Ecología, Estación Experimental de Zonas Áridas (EEZA-CSIC), 04120 Almería, Spain

<sup>d</sup> Instituto de Ciencias Químicas, Universidad Autónoma de Chile, 7500138 Santiago, Chile

<sup>e</sup> Departamento de Ecología y Geología, University of Málaga, 28071 Málaga, Spain

<sup>f</sup> Laboratoire de Géologie de l'Environnement et Ressources Naturelles, FS, Abdelmalek Essaïdi University, B.P. 2121, Mhannech II, 93002 Tetouan, Morocco

<sup>g</sup> Université Moulay Ismaïl, Laboratoire de Géologie Appliquée, Faculté des Sciences et Techniques, BP. 509, Bouslimane, 52000 Errachidia, Morocco

<sup>h</sup> Departamento de Mineralogía y Petrografía, University of Granada, 18071 Granada, Spain

<sup>i</sup> Departmentul de Geologie, Universitatea "Alexandru Ioan Cuza" din Iași, 20A, Carol I, 700505 Iași, Romania

<sup>j</sup> Departamento de Algebra, University of Granada, 18071 Granada, Spain

### ARTICLE INFO

#### Article history:

Received 1 March 2024

Accepted 3 March 2024

Available online 08 March 2024

Editor: Dr. Brian Jones

#### Keywords:

Foreland basins system

Tectono-sedimentary evolution

Miocene

Western External Rif

NW African margin

Maghrebian Ocean margins

### ABSTRACT

The Miocene evolution of the External Rif Zone (NW Africa Plate) was determined through multidisciplinary analysis of fourteen successions. The updated stratigraphic framework shows how Miocene sediments rest on the Cretaceous–Paleogene terrains through unconformity surfaces, whereas it rests with sedimentary continuity in two sectors. After recognition of lithofacies and three unconformities located near the Oligocene–Aquitian, Aquitanian–Burdigalian and Serravallian–Tortonian boundaries, the Miocene sedimentary record was divided into three stratigraphic intervals representing deep to shallow marine deposits as Aquitanian–Burdigalian, Langhian and Upper Serravallian–Missinian. The two oldest unconformities are restricted to the central sector, while the upper one is generalized and probably related to the nappe tectonics registered in all sectors of the External Rif. Data from analysis of tectofacies, petrology, mineralogy, meaning and implications of unconformities, and subsidence indicate that: (i) mass flow deposits (turbidites, slumps,olistostromes) are common in all successions but more frequent during the Lower Miocene; (ii) petrology of the detrital components of the arenites indicates recycled orogen-derived sediments, with quartz coming from erosion of metamorphic rocks of the Atlas orogen and/or the African craton; (iii) mineralogy of mudstones suggests a complex erosional evolution of local emerged areas derived from a mixture of contributions coming from the erosion of Upper Jurassic to Paleogene suites, and especially from kaolinite-rich Albian–Cenomanian to Paleogene successions with absence of a clear unroofing. The conjunction of all these clues reinforces the idea of a synsedimentary tectonics affecting the margin/basin system during the Miocene. A thickness analysis of the studied sedimentary successions allows proposing the evolution of the orogenic front and main depozones (foredeep, bulges, wedge-top and intramontane sub-basins) integrated in a complex foreland system migrating from north to south with the Atlas-Mesetas area acting as foreland during Miocene. The orogenic front moved from the Internal Intrarif to Mesorif and later to Internal Prerif. The main wedge-top basin also migrated from the Internal Intrarif to External Intrarif. The foredeep migrated from the Mesorif to the Internal Prerif, while the main forebulge was located in the External Prerif and a secondary bulge developed in the External Intrarif. Intramontane basins developed behind the orogenic front in relative extensional conditions moving from the Internal Intrarif to External Intrarif. The reconstructed Miocene evolution was inserted into a 2D paleogeographic-geodynamic evolutionary model using GPlates software, and then compared to those reported in other external margins of the western Tethys (Betic Chain, Tunisian Tell, Sicilian Maghrebids and Apennines), revealing important similarities and local differences.

© 2024 The Author(s). Published by Elsevier B.V. This is an open access article under the CC BY-NC license (<http://creativecommons.org/licenses/by-nc/4.0/>).

\* Corresponding author at: Departamento de Ciencias de la Tierra y del Medio Ambiente, Universidad de Alicante, Campus San Vicente, San Vicente del Raspeig, 03080 Alicante, Spain.  
E-mail address: [manuel.martin@ua.es](mailto:manuel.martin@ua.es) (M. Martín-Martín).

## 1. Introduction

The Alpine Rif Chain (western branch of north-Africa) is located in the NW portion of the African Plate (Fig. 1A). This chain is classically divided (Chalouan et al., 2008; Michard et al., 2008) into three main elements (Fig. 1B): (1) the Internal Zone, which derived from the Mesomediterranean Microplate (Guerrera et al., 2021); (2) the intermediate “Flysch Units” characterized by units resulting from the Maghrebian Flysch Basin (*MFB* hereafter) (Guerrera et al., 1993, 2005, 2021); and (3) the wide External Zone. The latter represent the deformed NW African margin (Martín-Martín et al., 2022a) and consist of Mesozoic to Miocene successions detached from their Paleozoic substratum (Atlas and Mesetas), and especially record the effects of the Cenozoic deformation related to the orogenic evolution of the Maghrebian Chain (Faccenna et al., 2001; Schettino and Turco, 2011; Carminati et al., 2012; Doglioni, 1992; Lustrino et al., 2013; Rossetti et al., 2013; Leprêtre et al., 2018; Guerrera et al., 1993, 2005, 2021). Based mainly on the structural position, Suter (1980a, 1980b) subdivided the External Rif Zone (*ERZ* hereafter) into three subdomains from N to S (Fig. 1B): Intraprif (mainly Cretaceous deposits), Mesorif (mainly Jurassic carbonate deposits to deep water turbidites), and Prerif (mainly made by Cenozoic olistostromes containing important fragments of ultrabasic rocks from a Triassic–Jurassic oceanic basement, Jurassic deposits derived from a carbonate platform, and Upper Miocene marly matrix containing Triassic basic subvolcanic rocks). In addition, the External Rif has been distinguished into western and eastern with respect to the Ketama “meridian” (Chalouan et al., 2008; Michard et al., 2008). The western one consists of sedimentary successions, while some of the eastern units show a slight metamorphism. A further subdivision of the “Intraprif” (Fig. 1B) has been recently proposed by Martín-Martín et al. (2022a) based on tectonic-unit criteria. In this way, the “Internal Intraprif” includes the following units: Internal Tangier, External Ketama-Tangier and Loukkos, while the “External Intraprif” would include the Cretaceous–Cenozoic El Habt and Ouezzane nappes overthrusting Mesorif and Prerif subdomains. The *ERZ* comprises a variety of stratigraphic and tectonic units from Trias to Miocene (Chalouan

et al., 2008). After Suter (1980a, 1980b), that proposed a modern geological framework of the Rif Chain, different local studies and models have been carried out in the *ERZ* (Lespinasse, 1977; Asebriy et al., 1987, 2003; Azdimousa et al., 2003, 2007; El Mrihiet et al., 2004; Tejera de Leon and Duée, 2003; Bargach et al., 2004; Zaghloul et al., 2005; Chalouan et al., 2008; Vázquez et al., 2013; Jabaloy-Sánchez et al., 2015; Maaté et al., 2017, 2018; Critelli, 2018; Abbassi et al., 2020, 2021, 2022; among many others; and references therein). Despite the several studies devoted to the *ERZ*, many problems are still unresolved and geodynamic reconstructions should be considered very hypothetical. The main problem is due to the lack of homogeneous data and the absence of interdisciplinary and extensive studies in this domain. Moreover, there are also interpretative difficulties relating to the pre-deformational position of many structural units. This paper is aimed at improving the knowledge of the Miocene tectono-sedimentary evolution of the western *ERZ* utilizing a homogeneous method, with a focus on the relationships between tectonics and sedimentation. To achieve this objective, this paper introduces an integrated multidisciplinary methodology, as follows: (i) integration of litho- and biostratigraphic findings; (ii) identification and datation of main unconformities and depositional sequences; and (iii) interpretation of petrological and mineralogical assemblages of detrital and mudstone suites, respectively. In order to frame the tectono-sedimentary evidence deduced from the previous analyses within the External Rif Zone evolution as a complex foreland system, the reconstructed geological evolution is used to create a 2D paleogeographic-geodynamic evolutionary model for the Rif Chain as whole. The GPlates basemap software is used for this target. For global integration criteria of our paleogeographic-geodynamic model, it is compared to models of other central-western Mediterranean margins (foreland basins systems) originated by the neo-Alpine Maghrebian tectonic evolution of the westernmost neo-Tethys during the Miocene. In view of the regional extension of the addressed topic, the interdisciplinarity methodology, and the previous investigations of the implicated sub-domains conducted by the same research group, the geological reconstruction meant to be a fundamental, updated framework of reference for the External Rif Domain at the Mediterranean scale.

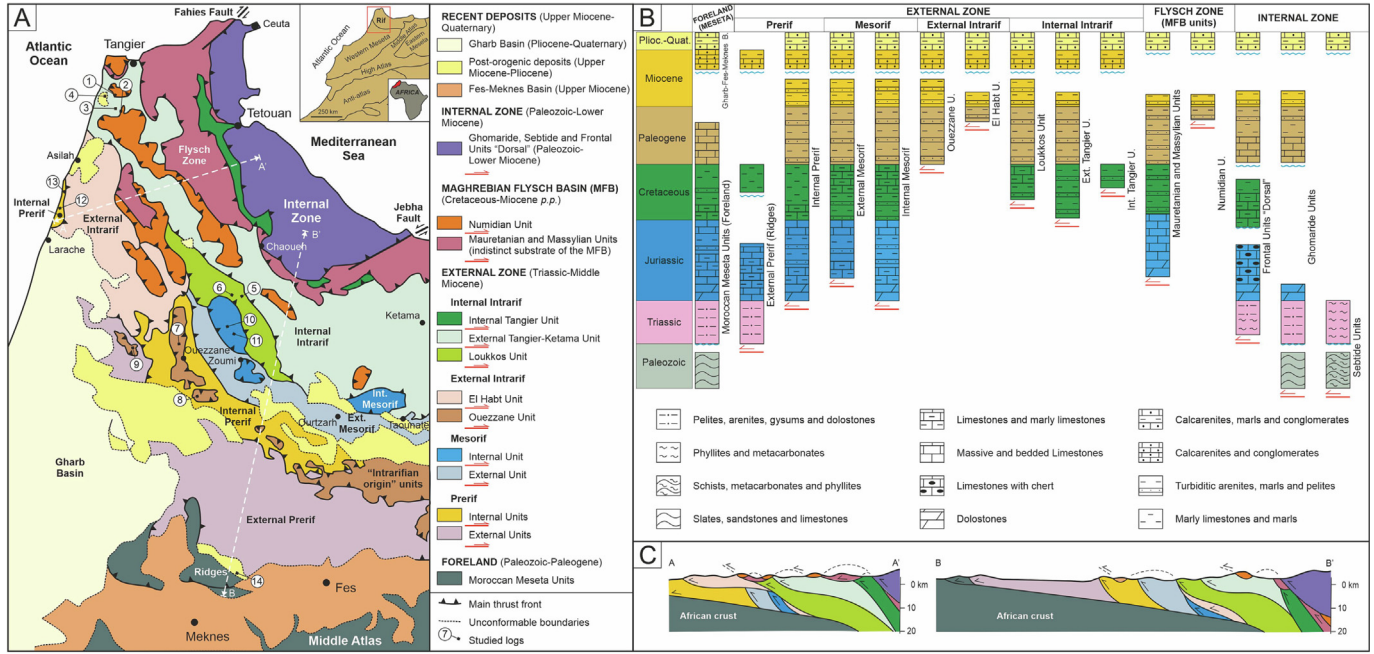


**Fig. 1.** Geological map of the Rif Chain. (A) Geological map of the Rif Chain showing the studied sectors and the location of the measured and studied stratigraphic successions (Logs) with an index sketch map of main domain of NW Africa (right-upper corner). (B) Geological information of the synthetic and most representative successions of the different domains and sub-domains of the Rif Chain. (C) Two schematic geological sections showing the study area structure.

## 2. Geological setting

The origin of the Rif Chain is linked to the alpine evolution of the westernmost Tethys and the subsequent opening of the Mediterranean together with the evolution of the western peri-Mediterranean chains (Doglioni, 1992; Guerrera et al., 1993, 2005; Doglioni et al., 1998, 1999; Michard et al., 2002; Chalouan et al., 2008; Guerrera and Martín-Martín, 2014; Critelli et al., 2017; Müller et al., 2018; among others). At the end of the Mesozoic, the African Plate was separated from the more northern Mesomediterranean Microplate through the MFB (western branch of the Maghrebian Ocean that was, in turn, the southern branch of the Tethys affected by the neo-Alpine evolution). The MFB would represent a connection between the Tethys and the Atlantic Ocean during the Meso-Cenozoic. The closure of the western MFB (Guerrera et al., 2021; Michard et al., 2002; Chalouan et al., 2008; Guerrera and Martín-Martín, 2014; Müller et al., 2018) would have happened mainly during the Miocene with the extrusion of the MFB-units and the propagation, in the time, of the deformation toward the External subzones. Previous models (Martín-Algarra, 1987; Doglioni, 1992; Guerrera et al., 1993, 2005; Guerrera and Martín-Martín, 2014; Critelli, 2018; among others) proposed the occurrence of a southern oceanic branch (Maghrebian Ocean, substrate of the MFB) in the central-western Mediterranean area affected by a Miocene evolution (neo-Tethys). In fact, the discovery at the base of the MFB of Jurassic ophiolite-type, basic rocks related to an oceanic crust (Durand-Delga et al., 2000; Boukaoud et al., 2021) with lateral oceanic branches in the External Rif Zones (Benzaggagh et al., 2013; Michard et al., 2014; Benzaggagh, 2016) confirms the described paleogeographic and paleotectonic evolutive framework. The chains originating from the tectonic-sedimentary evolution of this system extend from the Betic-Rifian Arc to the Calabro-Peloritano Arc with a partial extension in the southern Apennine (Belayouni et al., 2023b).

In particular, the ERZ would have behaved as a complex foreland basin system during a large part of Cenozoic, due to subduction beneath the Mesomediterranean Microplate (Guerrera et al., 1993; Abbassi et al., 2020, 2021, 2022). The tectono-sedimentary evolution of this system experienced different stages of subsidence due to a progressive Cenozoic deformation, where the Gharb Basin acted as the recent most portion of this complex foreland basin while the Atlas-Mesetas system worked as foreland (Michard et al., 2002; Chalouan et al., 2008). Contemporaneously, the roll-back of the subducting oceanic crust below the MFB would lead to the opening of the Mediterranean Sea as a back-arc basin during the late Oligocene (Royden, 1993). Benzaggagh et al. (2013) and Benzaggagh (2016) pointed out the presence of another oceanic branch between Intrarif and Mesorif (eastern External Rif Zone) by the occurrence of basalts, breccias and serpentinites rocks at the base of the External Intrarif units. This

reconstruction was considered by Martín-Martín et al. (2022a) as the most probably hypothesis considering the tectonic style of the External Intrarif units as extruded nappes similar to the units derived from the deformation of the Flysch Zone (MFB). Although the compression of the Tethyan domains began with the latest Cretaceous tectonic inversion (Stampfli and Kozur, 2006) causing folding during part of the Paleogene, the major compressive deformation proposed for the ERZ developed during the Miocene (Zakir et al., 2004; Chalouan et al., 2006) producing the structural architecture of nowadays (Fig. 2: Supplementary Material A1). This structuring consists in allochthonous thrusting units with south to west vergence (describe an arc: Fig. 2). Two of these units were extruded and override on other units as nappes (Flysch Zone and External Intrarif: Fig. 2). Furthermore, the strike-slip tectonics (Jebha and Fahies faults: Fig. 2) overprinted this Miocene deformation (Azdimousa et al., 2007). According to AïtBrahim et al. (2002), tectonics would have been accomplished in the Rif with a major compressional axis rotating approximately NE-SW to N-S during the Miocene. Many authors highlighted the tectonic complexity in the External Rif Zone, pointing out a nappe structure of units detached from their original paleogeographic position and overriding more external (Azdimousa et al., 2007; El Mrhiet et al., 2004; Bargach et al., 2004; Chalouan et al., 2008; Vázquez et al., 2013; Jabaloy-Sánchez et al., 2015). Despite recent studies devoted to the External Rif through interdisciplinary analyses (Maaté, 2017; Maaté et al., 2017, 2018; Martín-Martín et al., 2022a, 2022b, 2023), some issues still remain open.

## 3. Methods and analysis

As in previous publications targeting of similar topics (Martín-Martín et al., 2023), the used methodology includes: (1) Field analyses: detailed reconstruction of significant lithostratigraphic successions (Logs hereafter) in the considered area (Figs. 1 and 3), tectonic structures observations, and sampling; (2) Laboratory analyses: biostratigraphy and chronostratigraphy (Fig. 4), petrography of detrital lithofacies, and clay mineralogy of mudstones; (3) Computer data processing: treatment of results to carry out paleogeographic and paleotectonic reconstructions; and, (4) Reconstruction and interpretation of the main tectono-sedimentary events with an attempt at lateral correlation at a regional scale.

Planktonic foraminifera assemblages were determined on seventy-one samples (Logs 1–14) (Fig. 4) by using conventional methodology of washing and splitting by sieves of 150 µm (main studied fraction) and 125 µm. Reworked organic components were used to support the oldest age in cases of very poor or doubtful autochthonous microfauna or considered part of the detrital fraction. For biostratigraphic monitoring, specific Mediterranean Neogene zonation by Lirer et al. (2019), in combination with the more significant planktonic foraminiferal

External Rif Zone, Morocco

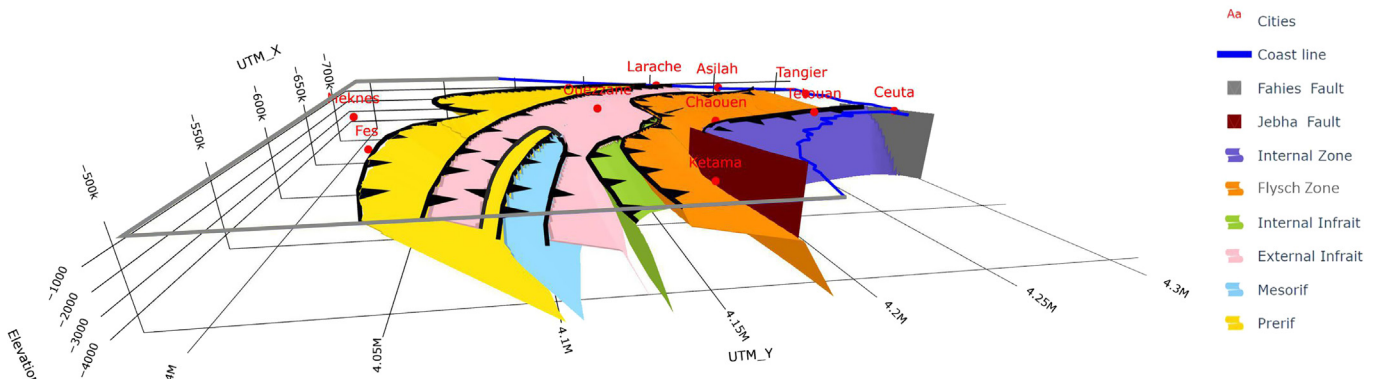
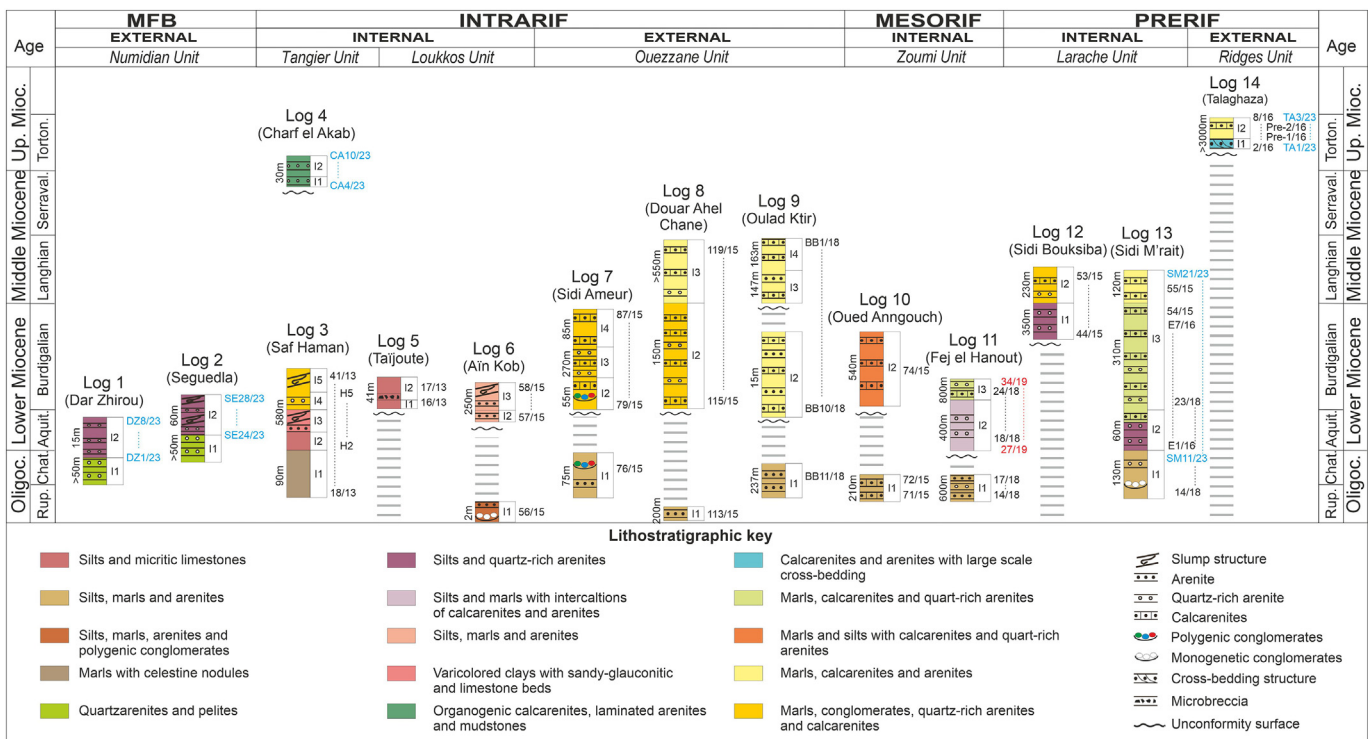


Fig. 2. Display of the 3D structural model performed with Python codes; see file 3D\_ZER\_structural\_model.HTML in Supplementary Material A1.



**Fig. 3.** Stratigraphic successions reconstructed in the: (i) External MFB (Numidian Unit: Log 1 Dar Zhirou and Log 2 Seguedla), (ii) Internal Intrarif (Tanger sector: Logs 3 Saf Haman and 4 Charf el Akab; Chaouen sector: Logs 5 Taïjoute and 6 Aïn Kob), (iii) External Extrarif (Ouezzane sector: Logs 7 Sidi Ameur, 8 Douar Ahel Chane and 9 Oulad Ktir), (iv) Mesorif (Zoumi sector: Logs 10 Oued Anngouch and 11 Fej el Hanout) and, (v) Prerif (Asilah sector: Logs 12 Sidi Bouksiba and 13 Sidi M'rabit; Ridges sectors: Log 14 Talaghaza), all located in the External Rif (Morocco) (Supplementary Material A2).

bio-events checked in the Mediterranean area by [Serrano \(1992\)](#) were considered, as well as correlated to the standard biozonation by [Blow \(1969\)](#). The biostratigraphic characterization of the Paleogene substratum was monitored by means of the biozonation of [Berggren and Pearson \(2005, 2006\)](#). For chronostratigraphic correspondence of the biostratigraphic intervals recognized, the Global Standard Chronostratigraphic Scale ([Lourens et al., 2004](#)) was used.

Thirty-six thin sections of different detrital materials from the most representative sections in the four studied subdomains ([Figs. 4 and 5](#)) were prepared and examined under polarizing microscope and applied to modal composition analysis. The schemes from [Folk \(1980\)](#), [Dunham \(1962\)](#) and [Zuffa \(1980\)](#) were used for nomenclature and classification. Framework mineral composition (modal analysis) was quantified using the point-counting method of Gazzi-Dickinson, as described by [Gazzi \(1966\)](#), [Dickinson \(1970\)](#) and [Ingersoll et al. \(1984\)](#). Sandstone framework components were divided into four petrographic groups defined by [Zuffa \(1980, 1985\)](#): (1) non-carbonate extrabasinal (NCE), (2) carbonate extrabasinal (CE), (3) non-carbonate intrabasinal (NCI), and (4) carbonate intra-basinal (CI). A Q-F-L<sup>\*</sup> ternary plot was used to classify sandstone types, L<sup>\*</sup> representing fine-grained rock fragments including CES. The petrofacies were represented in sandstone provenance diagrams as QmFLt (monocrystalline quartz, feldspar and lithic fragments) and Qmr/Qmo/Qp (monocrystalline quartz, undulosity <5°; monocrystalline quartz, undulosity >5°; polycrystalline quartz) following criteria of [Basu et al. \(1975\)](#), [Dickinson and Suckzeck \(1979\)](#), [Dickinson \(1985\)](#), and [Tortosa et al. \(1991\)](#).

Thirty-one samples of different clay-rich mudstones from the most representative sections in the four studied subdomains ([Fig. 6](#)) were examined by X-ray diffraction, including the whole-rock and <2 µm grain-size fraction (clay fraction hereafter). Samples were prepared according to methodology by [Croudace and Robinson \(1983\)](#), [Holtzapffel \(1985\)](#), and [Moore and Reynolds \(1997\)](#). A PANalyticalX'Pert Pro® diffractometer (Cu-K $\alpha$  radiation, 45 kV, 40 mA) equipped with an X'Celerator solid-state lineal detector was used to obtain diffractograms by a continuous

scan from 3° 2θ to 60° 2θ, with a 0.01° 2θ resolution. The Xpowder® program ([Martín-Ramos et al., 2012](#)) was used to evaluate the semi-quantitative mineral composition. The reflections and reflecting powers of [Schultz \(1964\)](#), [Biscaye \(1965\)](#), and [Holtzapffel \(1985\)](#) were used to identify and quantify the mineral phases. Replicate analyses of some samples gave a precision of ±3 % (2σ). Results are provided in weight percent, i.e., wt% normalized to 100 % with an accuracy of ~5 %. The ratio of intensities of the Qtz(001):Qtz(101) peak areas of quartz (Qtz(001):Qtz(101) ratio hereafter) ([Eslinger et al., 1973](#)), Sme(003):Sme(002) peak areas of smectite (Sme(003):Sme(002) ratio hereafter) ([Hunziker, 1986](#); [Drits et al., 1997](#); [Moore and Reynolds, 1997](#); [Moiroud et al., 2012](#)), and Ill(002):Ill(001) peak areas of illite (Ill(002):Ill(001) ratio hereafter) ([Hunziker, 1986](#); [Righi and Elsass, 1996](#); [Drits et al., 1997](#)) were determined in order to deduce the origin of inherited mineral phases from source areas that fed the basin and possible evidence of synsedimentary tectonics overprinting.

## 4. Results

### 4.1. Geological and stratigraphic framework

The units that characterize the External Rif are represented by typical margin successions but occasionally reduced units tectonically derived from the External portion of the MFB are also present. In particular, the most represented unit is the Uppermost Oligocene–Lower Miocene Numidian Fm usually in tectonic contact with different units of the External Rif Zone. More in detail, the Logs 1 and 2 reconstructed in the Tangier area consist in an alternation of thick and coarse quartz-rich turbidites and brownish-grayish pelites and marls alternating with thin quartzose turbidites of the Numidian Fm. Logs 3–6 reconstructed in the Internal Intrarif belong to the Tangier and Loukkos Units and represent the Miocene sedimentation affected by an important hiatus (Burdigalian–Serravallian p.p.). The older deposits represent

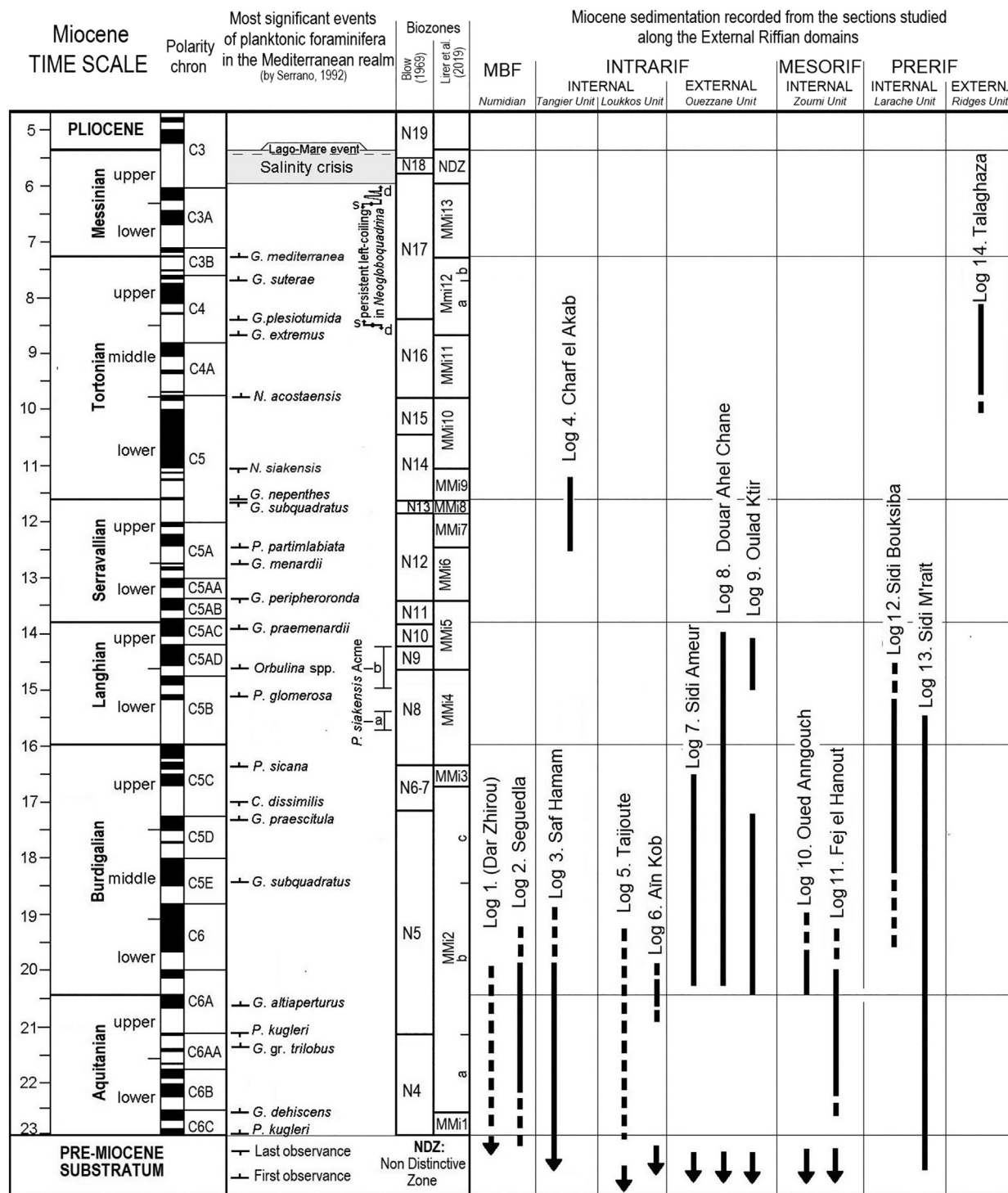


**Fig. 4.** Miocene time scale with the most significant events of planktonic foraminifera in the Mediterranean realm (Serrano, 1992) and the time range of the studied logs (Supplementary Material A3).

deep marine conditions (usually slope environment) with syntectonic features (mass flow deposits: olistostromes, turbidites, slumps, etc.). In turn, the younger ones (Log 4) represent a shallow marine platform. Logs 7–9 reconstructed in the External Intrarif belong to the Ouezzane Unit and represent the Burdigalian to lower Serravallian sedimentation. In general, a shallowing trend is recognized from deep marine (usually a continental slope environment) conditions with mass flow deposits to an external carbonatic platform (marls and calcarenites). Logs 10 and 11 reconstructed in the Zoumi Unit from the Mesorif represent the

Lower Miocene sedimentation. Again, deep marine conditions (usually slope) with syntectonic features (mass flow deposits) are registered. In the Internal Prerif the reconstructed Logs 12 and 13 belong to the Larache Unit representing the Lower–Middle Miocene sedimentation, also with deep marine conditions (usually slope) represented by mass flow deposits. Finally, the Log 14 from the “Prerifian Ridges” Unit was reconstructed in the External Prerif. This stratigraphic section only represents Tortonian shallow marine platform deposits evolving upwardly to external platform and deep basin.

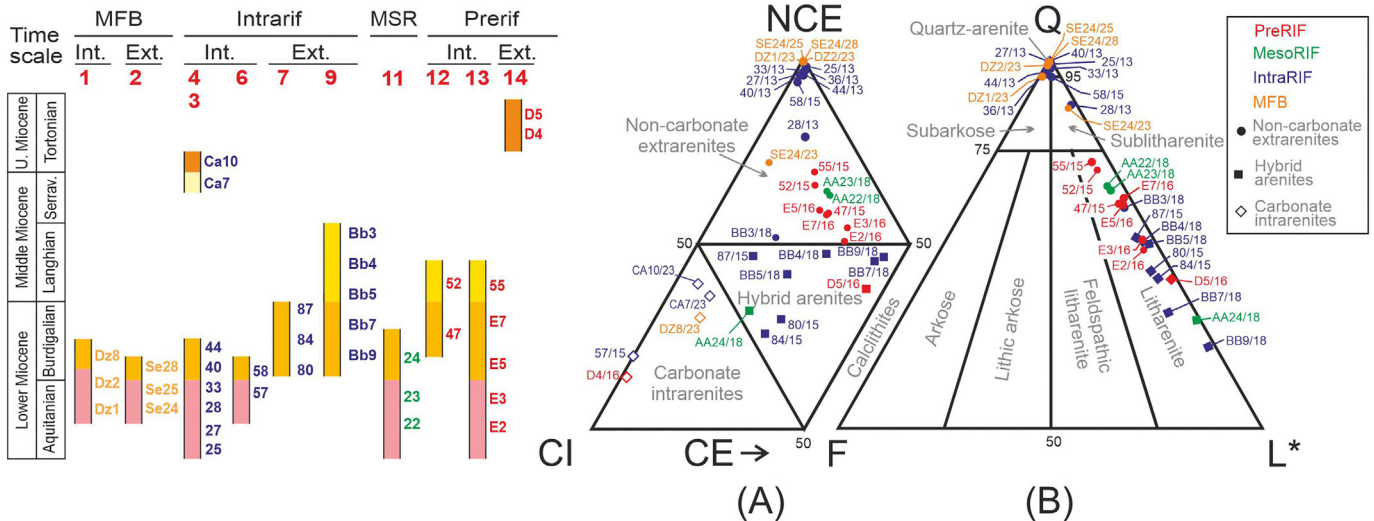


**Fig. 5.** Composition of Miocene detrital suites with indication of the studied sections and location of the samples: Logs 1 (Dar Zhirou) and 2 (Seguedla) in the Numidian Unit (External MFB); Logs 3 (Saf Haman) and 4 (Charf El Akab) in the Tanger Unit (Internal Intrarif Subdomain); Logs 7 (Sidi Ameur) and 9 (Ouled Kitir) in the Ouezzane Unit (External Intrarif Subdomain); Log 11 (Fej El Hanout) in the Zoumi Unit (Internal Mesorif Subdomain), Logs 12 (Sidi Bouksiba) and 13 (Sidi M'rabit) in the Larache Unit (Internal Prerif Subdomain), and Log 14 (Talaghaza) in the Ridges Unit (External Prerif Subdomain). (A) First-order compositional plot; NCE—non-Carbonate extrabasinal grains, CE—carbonate extrabasinal, and CI—carbonate intrabasinal. (B) Main composition plot; Q—quartz, F—feldspar, L\*—lithic fragments including carbonate rocks (Supplementary Material A4).

The selected fourteen Logs were analyzed and reconstructed based on detailed lithostratigraphic observations, and biostratigraphical and chronostratigraphical results. The location of each study Log is shown in Fig. 1, their stratigraphic reconstruction in Fig. 3, and their chronostratigraphy in Fig. 4. The complete stratigraphic description is reported in Table 1 and in Supplementary Material A2. Planktonic foraminifera information, including taxonomic formal names, appears in Supplementary Material A3. The following lithostratigraphic description is completed by biostratigraphic results arranged in subdomains according to the more recent subdivision (Martín-Martín et al., 2022a).

#### 4.2. Petrography

The petrographic analysis is referred to the detrital suites of the studied Logs from the External MFB and the ERZ. Location of the Logs and samples is shown in Fig. 3. Results of the modal point counting of the thirty-six studied samples are in Table 2; while modal ternary plots NCE-Cl-F and Q-F-L are represented in Fig. 5. Fig. 6 shows some polarizing microscope images with the most representative petrofacies. The samples coming from the MFB fall into the quartzarenite and sublitharenite fields of the Q-F-L plot (usually non-carbonate extrarenites in the NCE-Cl-F plot). They are mainly composed of monocrystalline quartz, calcite, dolomite and opaque minerals. The samples from the Internal Intrarif are quartzarenites and sublitharenites while those coming from the External Intrarif are litharenites.

All samples are usually intrarenites (grainstones/rudstones) (Fig. 6A), hybrid arenites (Fig. 6B, C) and extrarenites mainly composed by monocrystalline quartz and grains of glauconite and opaque minerals. Samples from the Mesorif are also litharenites (Fig. 6D) composed of quartz, sedimentary rock fragments (mudstone-wackestone, dolosparite) and bioclasts. Finally, samples from the Prerif (mainly extrarenites) are again litharenites (Fig. 6E) or hybrid arenites (Fig. 6F) made of quartz and sedimentary rock fragments (bioclastic grainstone-rudstone and mudstone-wackestone).

#### 4.3. Mineralogy

The mineralogical analysis provides the average whole-rock and clay fraction mineralogy of mudstones (Croudace and Robinson, 1983; Holtzapffel, 1985; Moore and Reynolds, 1997) of the studied thirty-one

samples (in wt%) coming from the Numidian Unit (External MFB, Log 2) and External Rif subdomains (Internal, Logs 3 and 4; External, Log 8; Mesorif, Log 11; and Prerif, Logs 13 and 14). Location of Logs and samples is shown in Fig. 3. Results are in Table 3, Fig. 7, and in Supplementary Material A5.

In detail, the MFB samples show an III+Kln  $\pm$  (I-S) + Sme clay-mineral association, while the dimensionless (S + K):I ratio by Daoudi et al. (1995) evidences an upwardly distality. Mature illite identifies supply from low-grade metamorphic rocks. The Internal Intrarif samples include III+Kln  $\pm$  (I-S) + Sme and Sme + (I-S)  $\pm$  III+Kln clay-mineral associations, while the (S + K):I ratio shows a decreasing distality from Aquitanian to Burdigalian and some increase during upper Serravallian-lower Tortonian. Inherited illite and dioctahedral smectite identify incipient low-grade metamorphism (anchizone) or weak burial diagenesis at most (Nieto et al., 1996; Lanson et al., 2009). The External Intrarif samples characterize III+Kln  $\pm$  (I-S) + Sme and III+(I-S)  $\pm$  Kln + Sme clay-mineral associations, while the (S + K):I ratio evidences a certain increasing distality from Burdigalian to Langhian. The Mesorif samples present III+Kln  $\pm$  (I-S) + Sme and III+(I-S)  $\pm$  Kln + Sme clay-mineral associations, while the (S + K):I ratio evidences a certain increasing distality during Early Miocene. The inherited character of the sediment supply seems also to increase during Early Miocene, including low-grade metamorphic rocks. The Internal Prerif samples include III+Kln  $\pm$  (I-S) + Sme and III+(I-S)  $\pm$  Kln + Sme clay-mineral associations, while the (S + K):I ratio decreases upwardly. Supply from incipient low-grade metamorphism (anchizone) or weak burial diagenesis is also observed. Finally, the External Prerif samples characterize the III+(I-S)  $\pm$  Sme + Kln clay-mineral association, while the (S + K):I ratio increases upwardly.

#### 5. Main unconformities and depositional sequences

The correlations of the reconstructed successions, together with their tectonic position in the considered sectors, allowed proposing a first stratigraphic framework of the Miocene stratigraphic record of the western ERZ based on sequence stratigraphy (Catuneanu et al., 2011) (Fig. 8). The reconstructed stratigraphy shows three unconformity surfaces, located approximately across (i) the Oligocene-Miocene boundary, with a gap covering the Upper Oligocene and/or

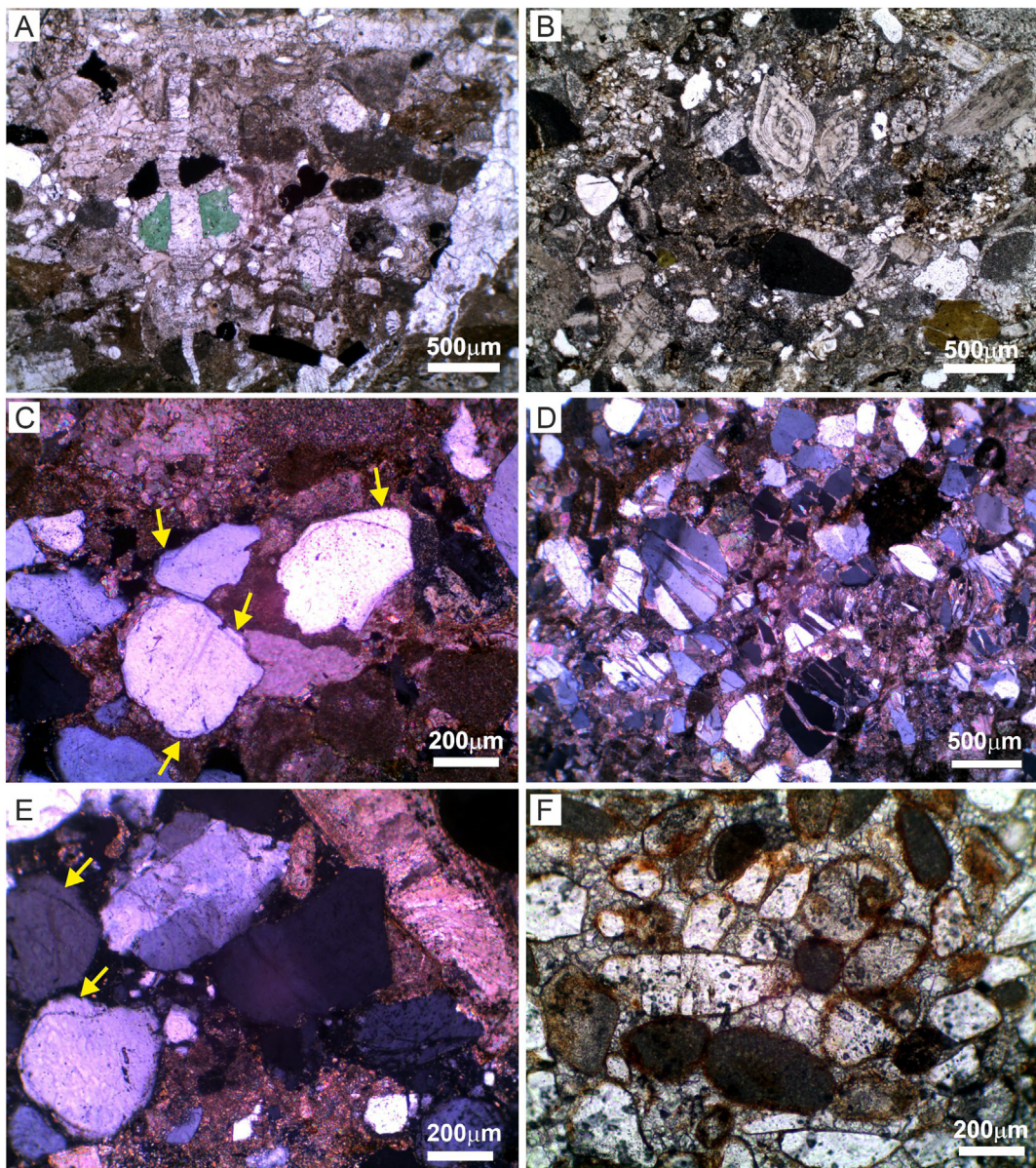


**Fig. 6.** Overall micrographs of the main studied petrofacies in thin section. (A) Sample 57/15: carbonate intrarenite (Burdigalian, Log 6: Ain Kob, Loukkos Unit, Internal Intrarif Subdomain), showing broken grains (bioclasts, glauconite and opaque minerals) related to calcite veinlets. (B) Sample 84/15: hybrid intrarenite (Burdigalian, Log 7: Sidi Ameur, Ouezzane Unit, External Intrarif Subdomain), showing poorly sorted quartz-rich grainstone composed of bioclast (mainly benthic foraminifers), quartz, lithoclasts, glauconite and opaque minerals. (C) Sample 87/15: hybrid intrarenite (Burdigalian, Log 7: Sidi Ameur, Ouezzane Unit, External Intrarif Subdomain), showing a well-rounded second-cycle quartz grain (arrows: inherit syntaxis cement). (D) Sample AA22/18: litharenite (Burdigalian, Log 11: Fej el Hanout, Zoumi Unit, Mesorif Subdomain), showing calcite veinlets and fractured grains (quartz, feldspar, opaque minerals). (E) Sample E2/16: litharenite (Aquitanian, Log 13: Sidi M'rāit, Larache Unit, Internal Prerif Subdomain), showing bioclasts and well-rounded second-cycle quartz grain (arrows: inherit syntaxis cement). (F) Sample D5/16: hybrid arenite (Tortonian, Log 14: Talaghaza, Ridges Unit, External Prerif Subdomain), showing moderately to well sorted quartz grains and carbonate lithoclasts, and ferruginous coatings. A-B-F—plane polarized light. C-D-E—cross polarized light (Supplementary Material A4).

the Aquitanian or even a part of the lower Burdigalian; (ii) the Burdigalian–Langhian boundary, only recognized in Log 9 (External Intrarif) with a gap affecting the upper Burdigalian; and (iii) the Middle–Late Miocene boundary, with a gap corresponding to the late Langhian–earliest Tortonian in most cases or even the whole pre-Tortonian Miocene time span as in Log 14 (External Prerif). The older unconformity is recognizable in almost all the examined sectors but in the Logs 1, 2 and 3 (External MFB and Internal Intrarif) and in the Log 13 (Internal Prerif). The intermediate unconformity is very local and only recognized in the Log 9 from the External Intrarif. On the other hand, the younger unconformity is again only recognized in the Logs 3–4 (Internal Intrarif) and Log 14 (External Prerif), corresponding in the other logs with the actual topographic erosive surface. Taking the

former into consideration, the two lowest unconformities can be referred to local tectonics, while the upper one is probably related to regional tectonics. Unconformities, lithofacies and sedimentary trends allow dividing the stratigraphic record into three Miocene depositional sequences (Catuneanu et al., 2011) referable in age to Aquitanian–Burdigalian, Langhian, and Tortonian–Messinian (Fig. 8). The first sequence is the best represented because recognized in the whole margin but in the External Prerif. The Langhian depositional sequence is represented in the External Intrarif and Internal Prerif, while the upper Serravallian–Tortonian is only represented in the Internal Intrarif and in the External Prerif. According to Miall (2016), the recognized gaps can be divided into depositional (unrecorded period above the most recent age of the lower stratigraphic unit) and/or erosional (unrecorded

**Table 1**

Lithostratigraphy.

Thick	Samples	Chronostratigraphy	Field Lithofacies description
Log 1, Dar Zhirou succession (65 m thick, Numidian Unit, External Maghrebian Flysch Basin/MFB)			
South foothills of the Jebel Dar Zhirou (UTM coordinates: 30S 238320 E-3951415 N)			
15	DZ1-8/23	Chattian-Aquitanian	Brownish-grayish pelites and marls, alternating with decimeter-sized thin and fine-grained quartz-rich (slightly cemented) of turbidite beds (Bouma sequences: Tc-e, Tc/e, and Td-e) and some calcareous turbidite beds.
50	-	Chattian	Coarse quartz-rich turbidite beds with brownish-grayish pelites and marls intercalations.
Log 2, Seguedla succession (110 m thick, Numidian Unit, External Subdomain of the Maghrebian Flysch Basin/MFB)			
East of Seguedla village (coordinates: 30S 241296 E-3946315 N)			
>20	SSE28/23	Aquitanian-Burdigalian	Brownish-gray mudstone with quartz-rich turbidite beds (up to 30 cm) showing parallel and convolute lamination (Tbc).
10	SE26-27/23		Brownish-gray mudstone with quartz-rich turbiditic beds (<25 cm) with parallel and convolute lamination (Tbc); some beds show big hypichnia (Zoophycos)
30	SE24-25/23		Brownish-gray mudstone with thin (<20 cm) rusty/brownish turbidite beds (mostly (Tbd) with epichnia (Scolicia), hypichnia (Paleodyction, Desmograp-ton, Planolites etc); mudstone contains sub-horizontal to vertical exichnia.
>50	-	Chattian	Coarse quartzarenites and conglomerates with thin brownish-grayish pelites (silt) and marls intercalations.
Log 3, Saf Haman succession (670 m thick, Tangier Unit, Internal Intrarif)			
North of Seguedla village (UTM coordinates: 30S 242,478 E-3947940 N)			
280	33/13-41/13, H5	Burdigalian	Quartz-rich arenites, frequent bioturbation; slump structure in the lower portion of the succession (75 m thick)
200	33/13-40/13, H4		Brownish (tobacco) silt and marls with intercalations of turbidite arenites and quartz-rich (glauconitic) beds (10–40 cm) with frequent bioturbation; follows a slump portion (about 100 m thick) of deformed varicolored silt with carbonate clasts ("Boules jaunes" Facies), black-gray marls, arenites and limestones.
10	28/13-32/13, H2, H3	Aquitanian-Burdigalian	Brownish silt and marls, thin turbidite arenitic beds, blackish-gray silt with micritic limestones and arenitic-glauconitic beds, all in a slump structure.
50	25/13-27/13		Varicolored clays with sandy-glauconitic bed, grayish lenticular limestones, homogeneous blackish-gray marls, silt with grayish limestones, sometimes grayish lenticular laminated limestones (10–20 cm thick) with bioturbation ( <i>Scolicia</i> sp.) and homogeneous black-gray marls; varicolored silt with grayish limestones in the middle-upper portion.
90	18/13-24/13, H1	Chattian-Aquitanian transition	Homogeneous blackish-gray marls with heavy celestine nodules.
Log 4, Charf el Akab succession (>30 m thick, Post orogenic Unit on Tangier Unit, Internal Intrarif)			
North of Lafarge Tangier plant (UTM coordinates: 30S 235931 E-3949504 N)			
2	CA9-CA10/23	Lower Tortonian-Upper Serravallian	Organogenetic calcarenites; thin cross-laminated arenites and yellowish-gray mudstones, calcareous-quartz-rich calcarenite/arenite beds (<10 cm) interlayered in yellowish mudstone.
2	CA7-CA8/23		Light gray mudstones.
10			Thicker calcarenites and arenites burrowed and bioclastic fragments of bivalves and pectinids; presence of "frosted" Qz grains.
6	CA5-CA6/23		Thin arenites (5–6 cm) of cross-laminated interlayered with mudstones
>10	CA4/23		Organogenic conglomerates (frequent fragments of echinoides and/or bivalves and pectinids), in the lowermost part, followed by bioclastic calcareous-quartz-rich with TCS (angular Qz grains). Underlying gap valued at approx. 6–7 Ma.
Log 5, Taijoute succession (41 m thick; Loukkos Unit, Internal Intrarif)			
South of Taijoute town (UTM coordinates: 30S 291256 E-3871093 N)			
21	16/13, 17/13	Upper Aquitanian-Lower Burdigalian	Brownish silt with micritic limestones.
Unconformity			
20		Middle Eocene	Microbreccia beds (1 m thick).
Erosive surface with gap of about 25–30 Ma.			
Silicified marls, grayish-black silt, micritic limestones (presence of Nummulitic layers); chaotic interval (slump) in the upper portion.			
Log 6, Aïn Kob succession (252 m thick; Loukkos Unit, Internal Intrarif)			
Near Aïn Kob village (UTM coordinates: 30S 284576 E-3870493 N)			
250	57/15, 58/15	Lowermost Burdigalian	Brownish silt and marls with thin arenite beds; chaotic interval (slump) in the upper portion.
Unconformity			
2	56/15	Chattian	Tectonized erosive surface with gap of about 6–7 Ma.
Mainly conglomerate, marls and calcarenite beds.			
Log 7, Sidi Ameur succession (485 m thick; Ouezzane Unit, External Intrarif)			
Near Sidi Ameur village (UTM coordinates: 30S 238815 E-3853994 N)			
85	80/15-87/15	Up to Upper Burdigalian	Stratified yellowish marls with intercalation of polygenic conglomerates and calcarenites (lower interval); turbidite quartz-rich arenites and calcarenites (intermediate interval); turbidite arenites (upper interval).
270			Erosive surface with gap of about 6–7 Ma.
55			Brownish silt, marls, arenites and interstratified polygenic conglomerate beds.
Unconformity			
75	76/15-79/15	Upper Chattian	
Log 8, Douar Ahel Chane succession (900 m thick; Ouezzane Unit, External Intrarif)			
Near Douar Ahel Chane village (UTM coordinates: 30S 263709 E-3863464 N)			
550	115/15-119/15	Upper Langhian	Whitish yellow marls and silt with intercalation of turbidite quartz-rich arenites (lower portion) and calcarenites (upper portion).
150		Lower Burdigalian	Stratified yellowish marls with intercalation of calcarenites, turbidite quartz-rich arenites and prevalent calcarenites beds.
Unconformity			
200	113/15	Middle Rupelian	Erosive surface with gap of about 10 Ma.
Brownish silt and marls with intercalation of turbidite arenite beds.			

**Table 1** (continued)

Thick	Samples	Chronostratigraphy	Field Lithofacies description
Log 9, Oulad Ktir succession (562 m thick; Ouezzane Unit, External Intrarif)			
Along Ktir river (UTM coordinates: 30S 273029 E-3828172 N)			
163	BB1/18-BB7/18	Langhian	Yellowish marls and silt with intercalation of calcarenites and turbidite quartz-rich arenites (lower interval); calcarenite beds (upper interval).
147			Erosive surface with gap of about 3 Ma.
Unconformity			
15	BB8/18-BB10/18	Middle Burdigalian	Yellowish marls and silt with intercalation of: calcarenites, turbidite arenites and conglomerate beds.
Unconformity			Erosive surface with gap of about 5 Ma
237	BB11/18	Lower Chattian	Yellowish silt and marls with intercalation of turbidite arenite beds
Log 10, Oued Anngouch succession (750 m thick, Zoumi Unit, Mesorif)			
Along Oued Anngouch (UTM coordinates: 30S 282874 E-3864901 N)			
540	73/15, 74/15	Burdigalian	Whitish and yellow marls and silt with prevailing intercalation of calcarenite beds.
Unconformity			Erosive surface with gap of about 6 Ma.
210	71/15, 72/15	Uppermost Rupelian Lower Chattian	Brownish (tobacco) silt and marls with intercalation of calcarenite beds.
Log 11, Fej el Hanout succession (1800 m thick, Zoumi Unit, Mesorif)			
from Fej el Hanout village to upper part of the Oued Anngouch (UTM coordinates: 30S 280451 E-3869737 N)			
800	AA18/18-AA24/18	Lower Burdigalian	Brownish marls with intercalations of calcarenites and turbidite (Ta-b; Tb-c) quartz-rich arenite beds.
400		Aquitanian	Brownish silt and marls with intercalations of calcarenites and turbidite quartz-rich arenite beds.
Unconformity			Erosive surface with a gap of about 4–5 Ma.
600	AA14/18-AA17/18	Uppermost Rupelian Lower Chattian	Brownish (tobacco) silt and marls with intercalation of turbidite arenitic and quartz-rich arenites beds.
Log 12, Sidi Bouksiba succession (580 m thick, Larache Unit, Internal Prerif)			
Near Sidi Bouksiba village (UTM coordinates: 30S 764874 E-3913183 N)			
230	44/15-53/15	Langhian	Whitish and yellowish marls and silt with intercalation of turbidite quartz-rich arenites and reworked calcarenite beds.
350		Burdigalian	Brownish silt with intercalation of turbidite quartz-rich arenites.
Log 13, Sidi M'rāït succession (620 m thick, Larache Unit, Internal Prerif)			
Near Sidi M'rāït village (UTM coordinates: 30S 764753 E-3918993 N)			
120	55/15, 33-34/19	Lower Langhian	Whitish-yellowish marls and silt with intercalation of calcarenite beds.
	SM20-21/23		
310	23/18, 54/15	Upper Burdigalian	Brownish (tobacco) marls with intercalations of prevalent calcarenites and subordinate turbidite quartz-rich arenites.
	30-32/19,		
	E1 to E7		
	SM16-19/23		
60	17-22/18	Aquitanian	Brownish silt with intercalation of turbidite quartz-rich arenites.
	27-29/19		
	SM11-15/23		
130	14-16/18	Chattian	Brownish silt and marls with intercalation of conglomerates and turbidite quartz-rich arenites.
Log 14, Talaghza succession (>3000 m thick, Ridges Unit; External Prerif)			
Near Talaghza village (UTM coordinates: 30S 279801 E-3769004 N)			
>3000	TA1-3/23	Middle-Upper Tortonian	Whitish-yellowish marls and silt with intercalation of calcarenite beds.
	2-8/16		Calcareous and arenites affected by cross-bedding at big-scale.
	Pre1/16, Pre2/16		
Unconformity			Erosive surface with an estimated gap between 50 and 60 Ma (affecting the Paleogene and Lower-Middle Miocene).

period below the oldest age of the upper stratigraphic one). The erosional gaps can be correlated with rising areas (regression) due to tectonics in the affected domains, while the depositional ones may be related to the transgressive onlap process covering a paleorelief created previously by tectonics. In the following [Section 6.2](#), the origin of these unconformities will be more discussed.

## 6. Evidence of syn-sedimentary tectonics

### 6.1. Mass flow deposits and faults

The mass flow deposits (turbidites, slumps, olistostromes) usually indicate ([Novak and Egenhoff, 2019](#); [Tek et al., 2020](#); among others) generation by a tectonic instability of the margin/basin system, and resedimentation of unstable material resulting from the erosion of a thrust front or nappe at the basin margin. Miocene turbidites are common in almost all the studied sectors, and often are associated with slumps and olistostromes ([Fig. 9A, B](#)). Slumps consist of deformed

intervals intercalated within not deformed deposits of the same lithofacies ([Tek et al., 2020](#)). They systematically appear in most of the studied successions ([Fig. 9C, D](#)) associated with turbidite successions. At certain stratigraphic levels, decametric deformed intervals are interpreted as large sliding masses. Olistostromes ([Condé, 2005](#)) interbedded within turbidite successions consist of coarse deposits (monogenic or polygenic conglomerates) usually showing a basal erosion surface and a poor internal organization ([Fig. 9E, F](#)) and normally constituted by extra-basinal supply. Although all these mass flow deposits could be also explained without synsedimentary tectonics, the confluence of all the elements here presented seems to indicate the tectonics as the most probably cause. Syn-sedimentary faults ([Tek et al., 2020](#)) are also common in almost all the observed outcrops, usually associated to mass flow deposits. These faults are sealed by undeformed or less deformed strata ([Fig. 9B](#)). The faults usually show a millimetric to centimetric displacement, which progressively reduces upward, and therefore are recognizable only in some layers covered by not faulted beds.

**Table 2**  
Petrological results.

	MFB						INTRARIF											
	External units						Internal units											
	Log 1			Log 2			Log 3						Log 4			Log 6		
	DZ1/23	DZ2/23	DZ8/23	SE24/23	SE24/25	SE24/28	25/13	27/13	28/13	33/13	36/13	40/13	44/13	CA7/23	CA10/23	57/15	58/15	
NCE	Qmr	45,12	47,76	10,57	23,23	45,88	46,05	39,88	30,90	20,64	34,86	29,93	29,95	29,98	13,83	15,93	6,33	31,60
	Qmo	35,38	36,56	1,76	7,62	36,13	37,40	44,12	45,15	24,06	46,76	41,67	47,25	34,73	7,91	8,41	1,43	43,54
	Qp2-3	-	-	0,88	0,37	-	-	-	-	0,54	0,28	-	-	-	1,19	1,33	-	0,14
	Qp > 3c	1,79	8,30	0,88	4,46	9,53	9,27	1,93	2,72	2,86	0,58	4,76	6,11	3,48	2,37	2,21	0,41	7,02
	Qp > 3f	0,18	-	2,20	1,30	0,18	-	-	-	0,68	1,46	0,77	1,56	0,96	0,79	0,88	-	0,49
	Qfrm	-	-	-	-	-	-	-	-	0,33	-	-	0,17	-	-	-	-	-
	Qfrg	-	0,18	-	-	-	-	-	-	-	-	-	-	-	-	-	-	-
	Qfrs	-	-	-	-	-	-	-	-	-	-	-	-	-	1,58	3,54	2,65	0,42
	Cq	-	-	7,49	6,51	-	-	0,20	0,22	-	-	0,34	-	-	2,77	3,10	3,88	1,05
	Ks	1,79	0,74	0,44	0,19	0,36	0,36	-	-	-	-	0,11	-	-	0,40	-	-	0,28
	Kfi	-	-	-	-	-	-	-	-	-	-	-	-	-	-	-	-	-
	Ck	-	-	0,44	0,74	-	-	-	-	-	0,10	-	-	-	-	-	0,41	0,63
	Ps	1,97	0,37	-	0,19	-	-	0,12	-	0,18	0,22	0,25	0,14	0,12	0,40	-	0,82	0,42
	Pfi	-	-	-	-	-	-	-	-	-	-	-	-	-	-	-	-	-
	Cp	-	-	-	-	-	-	-	-	0,10	0,12	0,13	-	-	-	-	0,61	0,28
	Ch	-	-	-	0,74	-	-	1,23	1,30	0,27	0,88	0,77	0,85	0,36	-	-	-	0,56
	Lm	-	-	-	0,37	-	-	0,10	-	-	-	-	-	-	-	-	-	0,21
	Ms	0,54	-	-	0,37	0,18	-	0,24	0,47	0,82	0,44	0,13	0,28	0,36	-	-	-	0,35
	HM	5,01	1,85	-	3,35	0,36	2,18	0,24	0,24	0,27	0,44	0,13	0,28	0,36	-	-	0,41	1,26
CE	Mi	-	-	1,32	-	-	-	0,49	0,47	4,22	1,14	1,90	1,65	0,12	1,19	-	-	-
	Sc	-	-	0,88	2,23	-	-	0,11	-	0,23	0,12	-	0,15	-	2,77	3,10	-	0,77
	Sd	-	-	-	1,30	-	-	-	-	1,02	-	-	-	-	-	-	-	0,49
	Fo	-	-	7,05	0,74	-	-	-	-	0,16	0,06	0,28	0,05	-	3,56	0,44	-	0,20
	Css	-	-	-	-	-	-	-	-	-	-	-	-	-	1,58	2,21	-	-
NCI	Ph	-	-	-	-	-	-	-	-	-	-	-	-	-	0,40	0,44	-	-
	Gl	3,22	1,29	1,76	8,18	1,98	1,45	0,97	3,78	8,32	0,73	1,42	3,27	0,96	1,58	1,33	1,02	2,81
	OM	0,58	0,14	4,85	6,88	0,20	0,04	1,09	1,06	2,18	0,73	0,39	0,71	1,68	3,16	2,21	5,10	2,67
CI	In	-	-	2,22	0,93	-	-	-	0,15	0,98	-	0,13	0,13	-	1,19	1,33	-	0,14
	Bi	-	-	12,33	4,09	-	-	0,24	0,32	5,02	-	0,90	0,72	0,36	18,97	28,76	51,02	0,42
Cm	Cm1	2,98	0,88	11,01	10,78	2,96	1,82	7,22	10,86	2,42	6,70	11,71	3,98	26,17	19,76	19,47	5,10	2,46
	Cm2	1,77	0,46	-	3,72	0,38	0,87	0,45	-	0,14	1,04	-	-	-	0,79	1,33	-	0,35
	Cm3	-	0,92	-	0,56	1,08	0,55	-	-	-	-	-	-	-	-	-	-	-
	Cm4	-	-	9,69	10,22	-	-	0,53	-	0,30	-	-	-	-	4,35	0,88	2,45	-
Ma		0,54	0,55	24,23	0,93	0,18	-	0,84	1,89	20,73	1,17	1,80	2,41	0,48	9,49	2,21	18,37	1,33
		100,00	100,00	100,00	100,00	100,00	100,00	100,00	100,00	100,00	100,00	100,00	100,00	100,00	100,00	100,00	100,00	

	MFB						INTRARIF											
	External units						Internal units											
	Log 1			Log 2			Log 3						Log 4			Log 6		
	DZ1/23	DZ2/23	DZ8/23	SE24/23	SE24/25	SE24/28	25/13	27/13	28/13	33/13	36/13	40/13	44/13	CA7/23	CA10/23	57/15	58/15	
NCE	96,05	98,67	24,67	53,72	99,61	98,50	96,81	93,45	69,46	96,88	94,03	92,84	95,75	24,67	36,73	16,94	88,62	
CE	-	-	9,25	4,28	-	-	0,66	0,54	7,71	1,48	2,59	1,98	0,16	9,25	5,75	0,00	1,54	
NCI	3,95	1,33	16,30	25,28	2,09	1,50	2,27	5,58	14,37	1,64	2,16	4,27	3,59	16,30	5,75	8,57	5,48	
CI	-	-	49,78	16,73	-	-	0,26	0,43	8,46	0,00	1,22	0,91	0,50	49,78	51,77	74,49	4,35	
	100,00	100,00	100,00	100,00	100,00	100,00	100,00	100,00	100,00	100,00	100,00	100,00	100,00	100,00	100,00	100,00	100,00	
Q	95,65	98,82	-	86,99	99,61	99,61	99,05	99,42	87,58	97,97	96,82	97,73	99,66	-	-	-	95,06	
F	4,35	1,18	-	2,23	0,39	0,39	0,14	-	0,48	0,51	0,48	0,16	0,17	-	-	-	1,83	
L*	-	-	-	10,78	-	-	0,68	0,58	11,93	1,52	2,70	2,10	0,17	-	-	-	3,11	
	100,00	100,00	-	100,00	100,00	100,00	100,00	100,00	100,00	100,00	100,00	100,00	100,00	-	-	-	100,00	
Qm	95,04	98,82	54,44	61,68	99,22	96,61	96,13	94,99	91,62	96,05	91,45	89,91	92,93	68,81	70,27	47,37	87,98	
F	4,34	1,18	2,22	1,63	0,39	0,38	0,14	-	0,58	0,51	0,50	0,17	0,18	1,83	-	5,92	1,70	
Lt	0,62	-	43,33	36,68	0,39	-	3,73	5,01	7,80	3,44	8,05	9,92	6,89	29,36	29,73	46,71	10,32	
	100,00	100,00	100,00	100,00	100,00	100,00	100,00	100,00	100,00	100,00	100,00	100,00	100,00	100,00	100,00	100,00	100,00	
Qmr	54,71	51,56	64,86	62,81	50,02	49,66	46,40	39,23	42,78	41,67	38,80	35,39	43,35	53,03	55,38	77,50	38,17	
Qmo	42,90	39,48	10,81	20,60	39,39	40,34	51,35	57,32	49,88	55,89	54,03	55,57	50,23	30,30	29,23	17,50	52,59	
Qp	2,39	8,96	24,32	16,58	10,59	10,00	2,25	3,45	7,34	2,44	7,17	9,04	6,42	16,67	15,38	5,00	9,25	
	100,00	100,00	100,00	100,00	100,00	100,00	100,00	100,00	100,00	100,00	100,00	100,00	100,00	100,00	100,00	100,00	100,00	

Results of the modal points count of the studied arenites using the Gazzi-Dickinson method. Abbreviations used for parameters of the modal analysis: NCE, non-carbonate extrabasinal clasts; Qmr, monocrystalline quartz with low undulosity <5°; Qmo, monocrystalline quartz with high undulosity >5°; Qp2-3, polycrystalline quartz: 2-3 subgrains; Qp > 3c, polycrystalline quartz: >3 subgrains; >0,062 µm; Qp > 3f, polycrystalline quartz: >3 subgrains; 0,030–0,062 µm; Qfrm, quartz in low/medium-grade metamorphic rock fragment; Qfrg, quartz in granite/gneiss rock fragment; Qfrs, quartz in sedimentary rock fragment; Cq, quartz grain replaced/corroded by carbonates; Ks, K-feldspar; Kfi, K-feldspar grain replaced by clay minerals; Ps, plagioclase; Pfi, plagioclase grain replaced by clay minerals; Ch, chert: >3 subgrains <0,030 µm; Lm, fine-grained sedimentary fragments; Ms, mica group minerals: mainly muscovite; Mfrm, mica in metamorphic rock fragment; CE, carbonate extrabasinal clasts; MI, micritic limestone fragments; Sc, sparite limestone fragments; Sd, dolosparite fragments; C, clayey clast; CI, carbonate intrabasinal clasts; In, micritic clasts; Bi, bioclasts; Cm, cements; Cm1, carbonate cement; Cm2, quartz and/or feldspar syntactic cement; Cm3, kaolinite and/or illite clay cement; Cm4, ferruginous cement; Ma, matrix; Q, total quartz; F, total feldspars; L\*, fine-grained rock fragments, including carbonate clasts.

INTRARIF								MESORIF				PRERIF										
External units								Internal units				Internal units										External units
Log 7				Log 9				Log 11				Log 12		Log 13				Log 14				
80/15	84/15	87/15	BB3/18	BB4/18	BB5/18	BB7/18	BB9/18	AA22/18	AA23/18	AA24/18	47/15	52/15	E2/16	E3/16	E5/16	E7/16	55/15	D4/16	D5/16			
9,44	5,69	18,61	17,09	15,46	13,09	10,36	6,09	29,41	28,40	8,38	26,12	30,21	15,55	16,72	26,04	25,09	31,59	5,63	19,96			
2,78	2,51	13,40	11,18	10,31	8,99	3,36	2,68	10,68	10,53	2,88	9,70	11,78	10,37	10,84	9,17	9,09	12,33	2,14	4,21			
0,28	-	1,24	0,64	0,44	0,26	0,56	-	0,96	0,83	-	0,93	0,91	0,81	0,58	0,71	1,09	-1,08	0,54	0,11			
1,94	0,91	0,74	-	-	-	1,68	1,12	5,76	5,33	1,05	7,84	5,29	4,49	5,07	7,94	8,55	4,62	-	2,88			
1,94	0,46	3,72	8,63	6,63	5,13	1,40	0,67	0,36	0,83	0,52	0,19	-	0,23	0,46	0,35	0,18	-	-	-			
-	-	-	-	0,74	0,64	-	-	-	-	-	-	-	-	-	0,35	0,18	-	-	-			
-	-	1,24	0,32	-	-	-	-	-	0,59	-	-	0,45	-	0,35	1,04	0,35	0,36	0,46	-	-		
6,67	9,34	2,98	2,24	1,91	1,67	6,16	8,95	0,96	1,07	8,90	0,37	-	-	-	0,53	0,55	-	2,41	0,55			
-	0,68	-	6,23	5,60	4,88	-	0,67	4,68	4,85	1,31	2,80	4,83	2,88	3,23	3,17	2,55	4,62	1,88	2,22			
-	0,91	0,99	0,16	0,15	0,13	-	1,12	0,24	0,47	0,79	0,19	0,45	0,92	0,69	0,53	-	0,77	-	0,44			
2,50	0,68	0,74	0,16	-	-	1,68	0,89	-	-	0,79	-	-	-	-	-	-	-	-	-			
-	-	-	-	-	-	0,56	-	0,84	0,59	-	0,56	0,76	0,58	0,46	0,35	0,55	0,77	-	0,22			
0,56	-	0,50	0,80	0,88	0,90	0,56	-	0,72	0,83	-	1,12	0,60	0,81	0,69	0,71	0,55	0,77	-	0,33			
0,56	-	-	0,32	0,29	0,26	0,56	-	-	-	-	-	-	-	-	-	-	-	-	-			
-	-	-	-	0,15	-	-	0,96	0,83	-	0,75	0,60	0,35	0,23	0,53	0,55	0,62	-	-	-			
0,83	0,46	-	1,12	0,88	0,64	0,56	0,67	0,96	1,07	0,79	1,31	0,60	0,35	0,81	1,41	1,64	1,08	-	0,33			
0,28	2,51	-	0,32	2,95	4,11	0,56	2,24	-	-	2,36	0,19	-	0,23	0,46	0,18	0,15	-	-	-			
-	0,68	0,50	-	-	-	0,45	0,84	0,59	0,79	-	-	-	-	-	-	-	-	-	-			
0,28	0,46	0,50	0,64	0,29	0,13	0,28	0,67	0,36	0,47	1,05	0,75	0,30	1,38	1,15	1,06	1,45	0,62	0,54	2,00			
11,11	15,95	14,89	18,37	18,85	18,61	11,76	14,54	7,44	6,98	10,99	13,62	6,80	3,46	3,92	13,23	12,73	6,16	1,34	11,64			
16,39	10,48	12,41	11,02	10,90	13,22	14,57	10,74	3,84	4,38	9,16	5,04	5,14	14,98	14,07	4,41	4,36	4,16	0,54	21,62			
-	-	-	-	-	-	0,56	-	4,56	4,14	-	0,56	0,30	1,50	1,15	0,53	0,55	0,46	-	1,33			
-	-	9,93	-	-	-	-	-	6,48	6,51	-	6,53	6,34	12,67	11,65	6,70	5,82	5,39	-	5,88			
-	-	-	-	-	-	-	-	-	-	-	-	-	-	-	-	-	-	-	0,44			
0,28	-	0,24	-	-	-	-	-	-	-	-	-	-	-	-	-	-	-	-	-			
4,17	2,96	2,24	0,48	0,74	0,67	4,76	3,36	1,56	1,78	4,19	0,56	1,21	-	-	1,06	0,91	1,69	0,80	-			
1,94	0,91	0,74	1,92	1,77	1,54	1,68	1,12	2,88	2,96	1,31	2,61	0,91	4,49	3,81	3,17	2,18	1,23	0,54	5,88			
2,22	0,68	-	0,13	-	-	1,68	0,89	0,96	0,83	1,05	1,68	0,76	2,07	1,73	1,41	1,64	1,08	-	1,66			
27,78	34,17	6,45	8,79	13,25	18,61	26,61	33,11	-	-	31,94	-	-	-	-	-	-	-	-	53,62	0,22		
5,83	7,52	6,70	6,39	5,89	5,13	6,44	7,16	9,00	9,23	8,12	12,50	11,93	11,52	9,80	11,46	12,73	10,32	26,81	11,64			
-	-	-	-	-	-	1,12	0,22	1,68	1,54	1,05	3,17	1,66	4,95	5,54	4,23	4,73	2,31	-	-			
-	-	-	-	-	-	-	0,45	-	-	-	2,72	3,11	3,46	-	-	2,31	-	-				
-	-	-	-	-	-	-	-	2,64	2,96	-	-	4,53	1,38	1,38	-	-	4,62	1,61	5,99			
2,22	2,05	1,24	1,76	1,47	1,28	2,52	2,24	1,20	1,42	2,62	0,93	0,91	0,58	1,04	1,41	1,82	0,77	1,61	0,44			
100,00	100,00	100,00	100,00	100,00	100,00	100,00	100,00	100,00	100,00	100,00	100,00	100,00	100,00	100,00	100,00	100,00	100,00	100,00	100,00	100,00		

INTRARIF								MESORIF				PRERIF										
External units								Internal units				Internal units										External units
Log 7				Log 9				Log 11				Log 12		Log 13				Log 14				
80/15	84/15	87/15	BB3/18	BB4/18	BB5/18	BB7/18	BB9/18	AA22/18	AA23/18	AA24/18	47/15	52/15	E2/16	E3/16	E5/16	E7/16	55/15	D4/16	D5/16			
28,06	25,28	45,16	50,00	46,69	40,82	29,41	26,85	59,42	58,82	30,63	55,97	61,18	47,35	51,44	56,61	57,27	64,10	13,14	33,26			
27,50	26,42	37,22	30,51	30,19	31,84	26,89	25,28	22,33	22,01	20,16	25,75	18,58	32,60	30,80	24,87	23,45	16,18	1,88	40,91			
6,39	3,87	3,23	2,40	2,50	2,31	6,44	4,47	7,08	7,69	5,50	3,17	6,65	5,88	5,19	4,23	3,09	7,55	2,95	11,86			
38,06	44,42	14,39	17,09	20,62	25,03	37,25	43,40	11,16	11,48	43,72	15,11	13,60	14,17	12,57	15,29	16,18	12,17	82,04	13,97			
100,00	100,00	100,00	100,00	100,00	100,00	100,00	100,00	100,00	100,00	100,00	100,00	100,00	100,00	100,00	100,00	100,00	100,00	100,00	100,00	100,00		
43,46	40,76	51,21	59,18	50,19	50,75	31,63	22,03	65,75	64,90	29,03	61,15	70,62	48,69	51,30	60,88	62,44	72,28	-	40,70			
4,71	4,27	3,33	2,86	1,92	2,63	6,12	1,76	3,50	3,48	1,61	3,36	3,22	3,76	2,88	2,55	2,20	3,90	-	1,38			
51,83	54,97	45,46	37,96	47,88	46,62	62,24	76,21	30,75	31,62	69,35	35,49	26,16	47,55	45,92	36,57	35,37	23,82	-	57,91			
100,00	100,00	100,00	100,00	100,00	100,00	100,00	100,00	100,00	100,00	100,00	100,00	100,00	100,00	100,00	100,00	100,00	100,00	100,00	100,00	100,00		
47,50	48,28	71,01	60,20	58,79	57,36	50,32	47,28	75,61	73,52	50,00	78,29	80,64	71,36	72,87	76,14	79,82	78,37	69,12	72,39			
8,13	4,02	4,35	2,30	2,51	2,49	7,64	4,89	3,98	3,88	3,49	4,28	3,64	5,49	4,04	3,41	2,75	4,19	0,00	2,41			
44,38	47,70	24,64	37,50	38,69	40,15	42,04	47,83	20,42	22,60	46,51	17,43	15,72	23,15	23,09	20,45	17,43	17,44	30,88	25,20			
100,00	100,00	100,00	100,00	100,00	100,00	100,00	100,00	100,00	100,00	100,00	100,00	100,00	100,00	100,00	100,00	100,00	100,00	100,00	100,00	100,00		
57,63	59,52	46,90	45,53	47,09	47,66	59,68	57,45	62,34	61,86	65,31	58,33	62,70										

**Table 3**

Mineralogical results.

Log	Age	Sample	Lithology	Whole rock					<2 μm grain-size fraction					(S + K):I		Qtz(100): Qtz(101)	Sme(003): Sme(002)	III(002): III(001)	
				Qtz	Phy	Cal	Dol	Kfs	Pl	Cpt	Sme	III	I-S	Kln	Chl	Pal			
2	Aquitanian	SE27/23	Silts	10	69	20	tr	tr	tr	5	39	16	32	8	0.94	0.29	1.17	0.31	
	Aquitanian	SE25/23	Silts	9	59	27	<5	tr	tr	<5	43	19	28	7	0.70	0.25	0.83	0.28	
3	Burdigalian	H4	Silts	22	50	18	8	tr	tr	tr	70	11	16	tr	tr	0.24	0.24	1.06	0.34
	Aquitanian	H3	Silts	19	48	30	<5	tr	tr	<5	73	8	17	tr	tr	0.26	0.24	1.03	0.51
4	Tortonian	CA8/23	Silts	10	70	19	tr	tr	<5	25	9	60	6	3.44	0.22	1.02	0.59		
	Serravallian	CA6/23	Silts	7	37	55	tr	tr	tr	6	31	27	34	<5	1.28	0.26	0.95	0.42	
8	Langhian	119/15	Marls	18	53	23	<5	<5	tr	<5	78	10	9	tr	0.15	0.23	0.98	0.34	
	Langhian	118/15	Marls	24	37	36	tr	<5	tr	6	76	11	7	tr	0.17	0.26	0.95	0.33	
	Langhian	117/15	Marls	15	35	47	tr	<5	tr	<5	78	9	11	tr	0.17	0.33	0.86	0.36	
	Burdigalian	116/15	Marls	30	47	22	tr	tr	tr	81	10	8	tr	0.11	0.22	0.91	0.33		
	Burdigalian	115/15	Marls	10	44	44	<5	tr	tr	5	83	7	5	tr	0.12	0.28	0.92	0.39	
11	Burdigalian	34/19	Marls	14	69	<5	tr	10	<5	5	26	26	43	tr	1.85	0.28	0.84	0.56	
	Burdigalian	33/19	Marls	14	63	13	<5	7	tr	<5	51	14	29	<5	<5	0.61	0.26	1.52	0.41
	Burdigalian	32/19	Marls	13	74	11	tr	tr	tr	<5	43	21	30	<5	tr	0.77	0.25	1.47	0.42
	Burdigalian	31/19	Marls	10	58	29	tr	<5	tr	tr	58	17	16	8	tr	0.29	0.27	1.56	0.48
	Burdigalian	30/19	Marls	14	67	10	<5	tr	5	tr	64	14	12	6	<5	0.20	0.26	1.46	0.39
	Aquitanian	29/19	Marls	12	59	21	tr	5	<5	<5	53	17	13	14	tr	0.28	0.26	1.32	0.31
	Aquitanian	28/19	Marls	16	67	14	tr	<5	tr	<5	61	17	19	tr	0.34	0.26	1.31	0.36	
	Aquitanian	27/19	Marls	12	61	24	tr	<5	tr	<5	62	19	14	tr	0.29	0.26	1.19	0.35	
13	Langhian	SM20/23	Marls	10	59	28	<5	tr	tr	9	48	27	16	tr	0.52	0.29	0.81	0.51	
	Langhian	SM19/23	Marls	10	55	27	<5	tr	<5	tr	5	56	23	15	tr	0.36	0.23	1.07	0.36
	Burdigalian	SM18/23	Marls	8	49	42	tr	tr	<5	75	14	8	tr	0.13	0.28	0.94	0.39		
	Burdigalian	SM17/23	Marls	6	57	31	<5	tr	<5	<5	45	15	37	tr	0.89	0.21	1.16	0.36	
	Burdigalian	SM16/23	Marls	7	89	tr	<5	tr	<5	7	29	22	42	tr	1.69	0.26	1.05	0.36	
	Aquitanian	SM14/23	Silts	9	83	5	tr	<5	tr	5	11	18	66	tr	6.45	0.27	1.11	0.39	
	Aquitanian	SM12/23	Silts	11	74	10	tr	<5	<5	7	13	21	56	<5	4.85	0.28	0.95	0.36	
	Aquitanian	SM11/23	Silts	10	74	12	<5	tr	tr	6	19	20	53	<5	3.11	0.24	1.09	0.35	
14	Tortonian	TA3/23	Marls	<5	20	75	<5	tr	tr	<5	35	40	8	13	0.11	0.24	0.82	0.29	
	Tortonian	TA2/23	Marls	<5	14	84	tr	<5	tr	<5	51	41	tr	5	0.04	0.29	0.89	0.44	
	Tortonian	TA1/23	Silts	5	20	68	5	<5	tr	<5	49	35	<5	5	0.08	0.29	0.92	0.40	

Average whole-rock and <2 μm grain-size fraction mineralogy (in wt%) of samples from Log 2 (Seguedla) in the Numidian Unit (External Maghrebian Flysch Basin), Log 3 (Saf Haman) and Log 4 (Charf El Akab) in the Tangier Unit (Internal Intrarif Subzone), Log 8 (Douar Ahel Chane) in the Ouezzane Unit (External Intrarif Subzone), Log 11 (Fej El Hanout) in the Zoumi Unit (Internal Mesorif Subzone), Log 13 (Sidi M'r'ait) in the Larache Unit (Internal Prerif Subzone), and Log 14 (Talaghaza) in the Ridges Unit (External Prerif Subzone). tr, traces; Qtz, quartz; Phy, phyllosilicates; Cte, calcite; Dol, dolomite; Kfs, K-feldspar; Pl, plagioclase; Cpt, clinoptilolite; Sme, smectite; Ill, illite; I-S, random mixed layer illite-smectite; Kln, kaolinite; Chl, chlorite; Pal, palygorskite; dimensionless (smectite+kaolinite):illite ((S + K):I) ratio; and intensities ratio of the Qtz(001):Qtz(101) peak areas of quartz, Sme(003):Sme(002) peak areas of smectite under ethylene glycol solvation, and Ill(002):Ill(001) peak areas of illite.

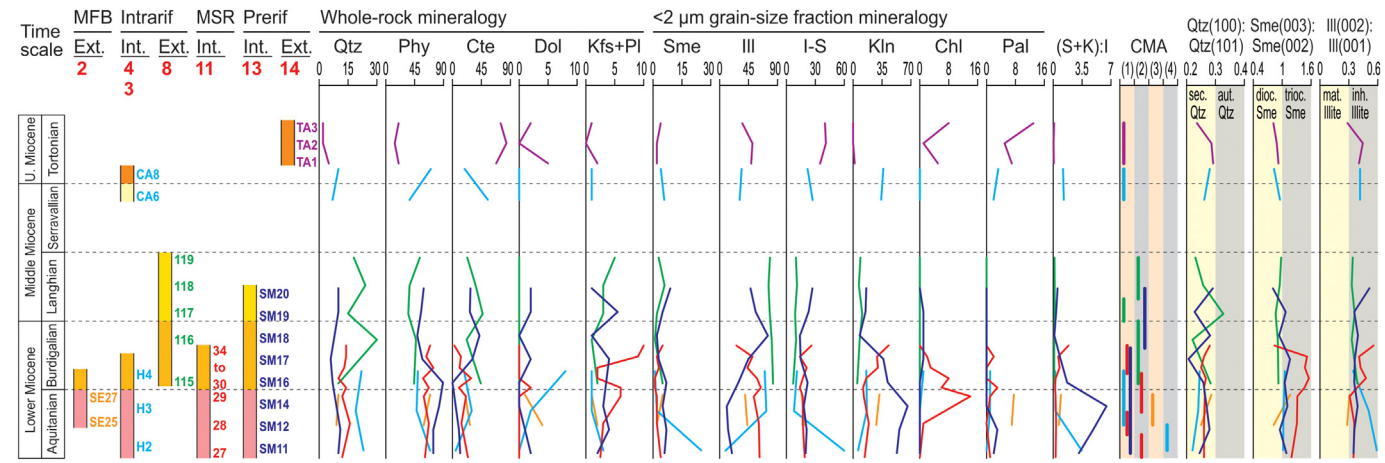


**Fig. 7.** Mineralogy of mudstones from (Fig. 2) with indication of the studied sections and location of the samples: Log 2 (Seguedla) in the Numidian Unit (External MFB), Log 3 (Saf Haman) and Log 4 (Charf El Akab) in the Tanger Unit (Internal Intrarif Subdomain), Log 8 (Douar Ahel Chane) in the Ouezzane Unit (External Intrarif Subdomain), Log 11 (Fej El Hanout) in the Zoumi Unit (Internal Mesorif Subdomain), Log 13 (Sidi M'r'ait) in the Larache Unit (Internal Prerif Subdomain), and Log 14 (Talaghaza) in the Ridges Unit (External Prerif Subdomain). The results for the whole rock and the <2 μm grain-size (clay) fraction are expressed in wt%. It has also displayed the dimensionless (smectite+kaolinite):illite ((S + K):I) ratio; the recognized clay-mineral associations (CMA) as mixtures from Upper Jurassic to Paleogene clay mineral assemblages as (1) Upper Jurassic and Lower Cretaceous [Ill+Kln ± (I-S) + Sme], (2) Albian to Paleogene [Ill+(I-S) ± Kln + Sme], (3) Upper Cretaceous [Sme + (I-S) ± Ill+Kln], and (4) Upper Cretaceous to Paleogene [Ill+(I-S) ± Sme + Kln]; and the intensities ratio of the Qtz(001):Qtz(101) peak areas of quartz, Sme(003):Sme(002) peak areas of smectite from ethylene-glycol solvated clay-fraction, and Ill(002):Ill(001) peak areas of illite. Qtz—quartz, Phy—phyllosilicates, Cte—calcite, Dol—dolomite, Kfs—K-feldspar, Pl—plagioclase, Sme—smectite, Ill—illite, I-S—random mixed layer illite-smectite, Kln—kaolinite, Chl—chlorite, Pal—palygorskite, sec—secondary quartz, aut—authigenic quartz, dioc—diotahedral smectite, trioc—trioctahedral smectite, mat—mature illite, and inh—inherited illite (Supplementary Material A5).

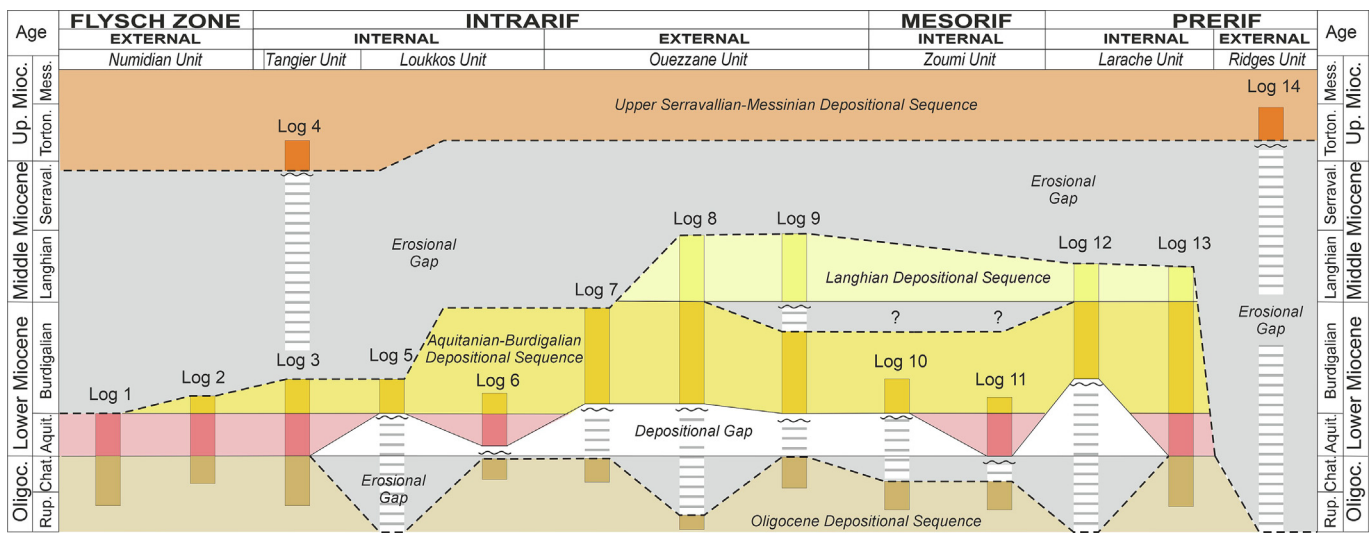


**Fig. 8.** Miocene stratigraphic framework of the western External Rif Zone, showing stratigraphic units, unconformities, and depositional vs erosional gaps.

## 6.2. Unconformities implications on synsedimentary tectonics

As presented above, the studied stratigraphic record is characterized from unconformities of different origin. Some of them seem to match with regional deformation phases affecting the western Tethys, which are widely mentioned in the literature (Martín-Algarra, 1987; Maaté, 1996; Khomsi et al., 2006, 2009; Michard et al., 2002; Chalouan et al., 2008; Guerrera and Martín-Martín, 2014; Guerrera et al., 2021). Thus, the unconformity across the Oligocene/Miocene boundary corresponds with a local tectonic phase mentioned in literature and related to a flexural deformation of the Atlas front as a forebulge of the foreland basin system (Khomsi et al., 2006, 2009). The unconformity near the Lower–Middle Miocene boundary is coincident with the end of structuring of the Internal Rif Zones, the closure of the MFB and the extrusion of the Flysch nappes (Martín-Algarra, 1987; Maaté, 1996; Michard et al., 2002; Chalouan et al., 2008; Guerrera and Martín-Martín, 2014; Guerrera et al., 2021). Finally, the younger unconformity is contemporary with the propagation southward of the tectonic nappes in the ERZ (Michard et al., 2002; Chalouan et al., 2008; Abbassi et al., 2020). The good agreement of unconformity with well-known tectonic phases in the areas reinforces the idea of a probably contemporary synsedimentary tectonics. All these tectonic events affecting the Miocene successions (Michard et al., 2002; Chalouan et al., 2008; Guerrera and Martín-Martín, 2014) can refer to the neo-alpine or Maghrebian phase (Guerrera et al., 2021). This phase is regionally linked to the closure of the southern branch of the western Tethys (MFB; Michard et al., 2002; Chalouan et al., 2008; Guerrera and Martín-Martín, 2014), which would originate the Maghrebian Chain (Rif, Tell and Calabria-Peloritani Arc), as well as most of the Betic Cordillera.

## 6.3. Petrographical evidence

Modal analyses of samples corresponding to the External MFB indicate middle- to high-grade metamorphic source, while the Internal Intrarif indicate low metamorphic source areas for the extrabasinal quartz grains (Dickinson et al., 1983; Dickinson, 1985) (Fig. 10). Both MFB and Internal Intrarif samples plot into the “Craton interior”, and minorly in the “transitional recycled orogen” tectonic setting evidencing a main supply from a craton under erosion (Dickinson et al., 1983; Dickinson, 1985). Both source area and tectonic setting are coincident with the hybrid arenites and sandstones (extrarenites) in the External Intrarif and derived from the erosion of a “transitional recycled” setting (Dickinson et al., 1983; Dickinson, 1985) indicating sediments derived

from collisional orogens (Fig. 10). In the rest ERZ (Mesorif and Prerif) modal analyses of sandstone samples, both extrarenites and hybrid arenites, indicate middle to upper rank metamorphic source areas (sedimentation during tectonic rising) for the extrabasinal quartz grains (Basu et al., 1975; Tortosa et al., 1991) (Fig. 10) falling into the “quartzose recycled orogen” tectonic setting (Dickinson et al., 1983; Dickinson, 1985). The intrabasinal grains must be derived from erosion of the local limestone substrate and areas with active benthic carbonate production. Locally, where hybrid arenites dominate (External Prerif), both coeval and non-coeval carbonate sedimentary sources must be more important. In both Mesorif and Prerif Subzones, in contrast to the Internal Intrarif the presence of features of recycling processes, such as the existence of second-cycle or recycled quartz grains and the relative abundance of sedimentary rock fragments suggests an origin related to the erosion of older siliciclastic and carbonate formations (Zuffa, 1987; Critelli et al., 2003; Garzanti, 2017; Critelli, 2018). The abundance of monocrystalline quartz (with evidence of recycling), the scarce presence of unstable minerals (feldspars, micas), and the presence of ultra-stable heavy minerals (zircon) also point to a multicycle origin derived very probably from the African Craton and the Variscan Atlas Chain in tune with paleogeographic position of the basins. Several repeated erosion-sedimentation cycles are also inferred for the terrigenous petrofacies (represented by mature quartzarenites and sublitharenites) in the MFB and Internal Intrarif.

## 6.4. Mineralogical evidence

The clay mineral associations recognized in the Aquitanian to Tortonian lithofacies (Fig. 7) are analogous to those reported in other detrital aluminic-magnesian-rich Miocene marine sediments of the western Tethys (Biscaye, 1965; Chamley, 1989; Chamley et al., 1986; Pletsch, 1997; Alcalá et al., 2001, 2013a, 2013b; Maaté et al., 2017; Abdelmalek et al., 2017; Martín-Martín et al., 2018). They are considered mixtures of clay mineral assemblages supplied from well documented External Rifian Jurassic to Paleogene suites (Pletsch et al., 1996; Pletsch, 1997; El Ouahabi et al., 2014; Faleh and Sadiki, 2002; Maaté et al., 2017; Martín-Martín et al., 2022a, 2023), that vary from bottom to top of the successions and among them, allowing deductions of the source areas evolution and synsedimentary tectonic episodes overprinting the predominant inherited mineralogy. Regarding the source areas evolution, in the Internal Intrarif (Tangier Unit) the Aquitanian and lower Tortonian clay mineral

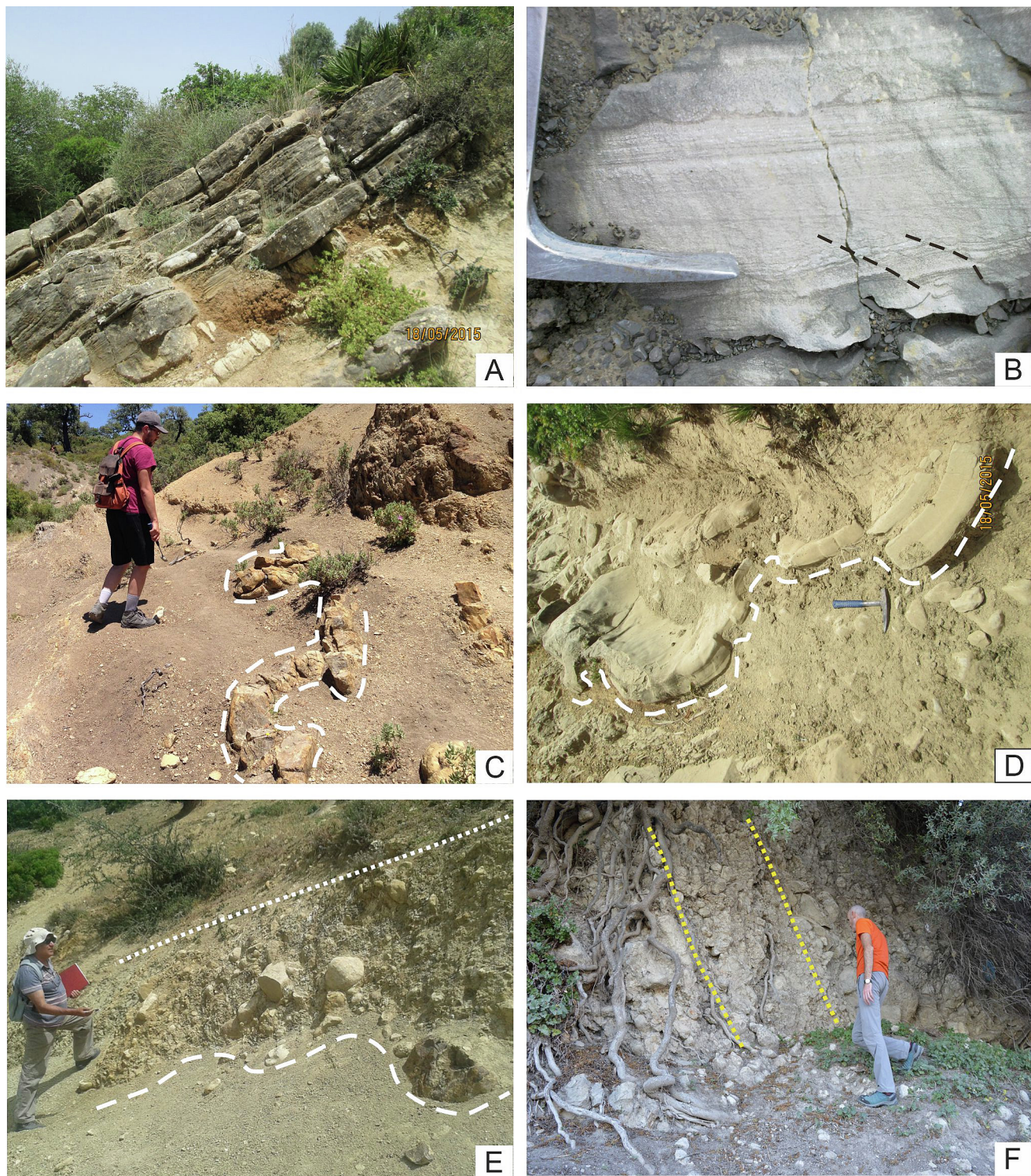


**Fig. 9.** Sedimentary and tectonic structures supporting synsedimentary tectonics. (A) Langhian turbidite (Log 8, Douar Ahel Chane). (B) Aquitanian turbidite with synsedimentary small faults (Log 3, Saf Haman). (C) Aquitanian slump (Log 6, Ain Kob). (D) Langhian slump (Log 8, Douar Ahel Chane). (E) Burdigalian mass flow (Log 8, Douar Ahel Chane). (F) Burdigalian mass flow (Log 9, Oulad Ktir).

associations (Fig. 7) identify a main sediment supply of illite-rich Upper Cretaceous and Paleogene suites. In the External Intrarif (Ouezzane Unit) supply during Burdigalian and Langhian (Fig. 7) mostly comes from kaolinite-rich Albian–Cenomanian and smectite-rich Upper Cretaceous suites (Fig. 11). In the Mesorif (Zoumi Unit) sources areas during Aquitanian and Burdigalian are similar to that proposed in the External Intrarif but acting in different times (Fig. 11), while the

presence of chlorite identifies additional supply of Upper Jurassic and Lower Cretaceous rocks (Azdimousa et al., 2003; El Ouahabi et al., 2014). In the Internal Prerif (Larache Unit) the Aquitanian to Langhian clay mineral associations (Fig. 7) suggest mixtures of Albian–Cenomanian and Paleogene suites (Fig. 11). In the External Prerif (Ridges Unit) the Tortonian clay mineral association (Fig. 7) identifies supply of Albian–Cenomanian suites with some additional supply of

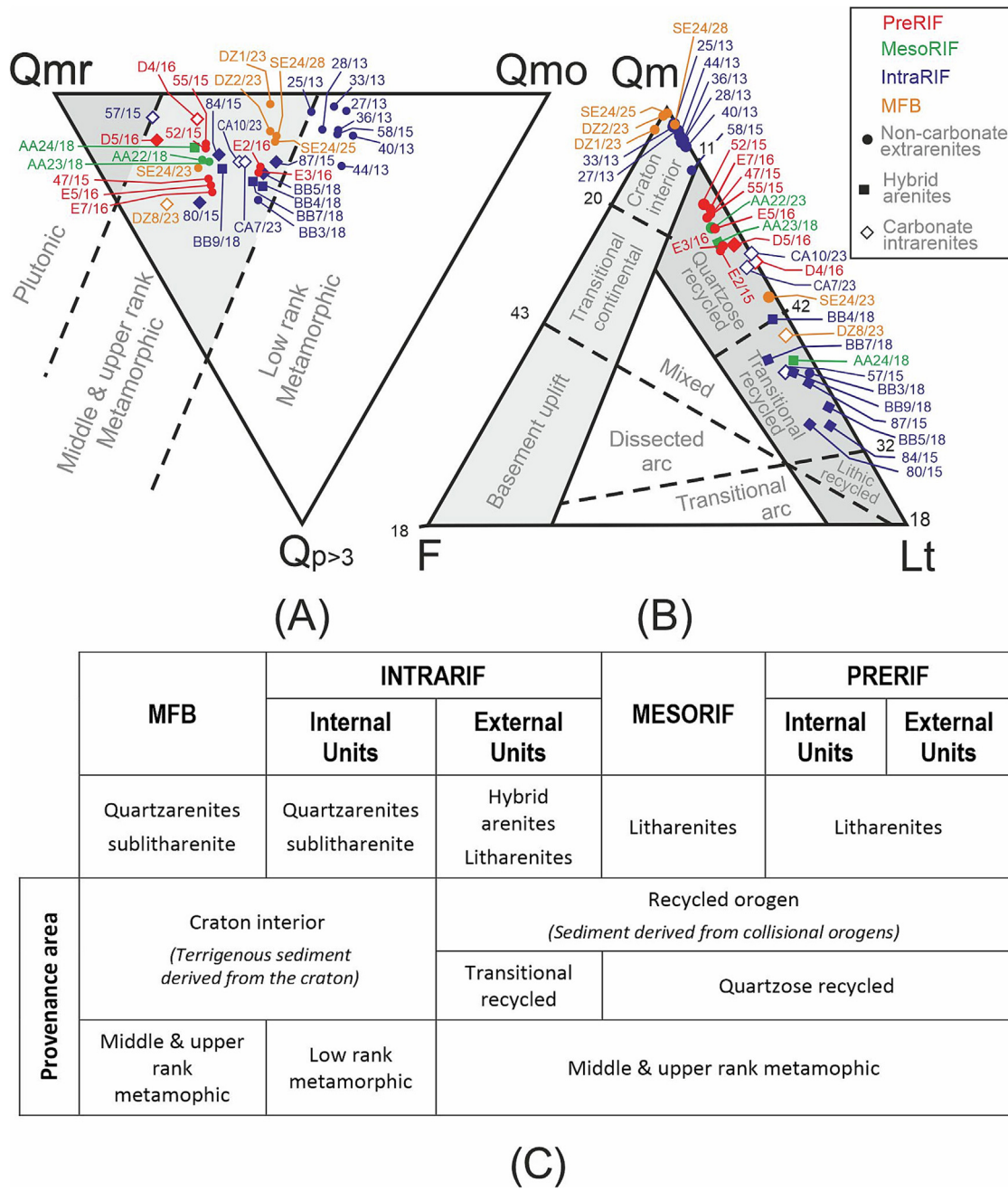


**Fig. 10.** Sandstones provenance diagrams. (A) Qmr/Qmo/Qp ternary diagram (Basu et al., 1975; Tortosa et al., 1991); Qmr—monocrystalline quartz, undulosity <5°; Qmo—monocrystalline quartz, undulosity >5°; Qp—polycrystalline quartz; (B) Qm/F/Lt ternary provenance discrimination diagram (Dickinson et al., 1983); Qm—monocrystalline quartz; F—plagioclase and K-feldspars; Lt—lithic fragments including carbonate extrabasinal clasts (CE); (C) classification, source origin and metamorphic rank of the quartz grains of the studied samples according to their respective sub-domains.

Upper Jurassic and Lower Cretaceous rocks. In the External MFB the Aquitanian clay mineral association (Fig. 7) indicates a predominant supply from Paleogene suites (Fig. 11). In terms of proximality-distality for source areas and evidence of syn-sedimentary tectonic overprinting the inherited mineralogy, the Intrarif and Prerif seem to be the distalmost areas during Aquitanian (higher (S + K):I ratios; Fig. 7). It is in good agreement with the existence of an oceanic branch in the External Intrarif–Mesorif boundary area (Benzaggagh et al., 2013; Benzaggagh, 2016; Michard et al., 2014, 2018). During early Burdigalian, distality decreases (lower (S + K):I ratios; Fig. 7) in the whole area. In the Intrarif and Mesorif, the increasing terrigenous supply indicates a tectonic reactivation of reliefs with distalmost areas in

the Intrarif. During Langhian, distality increases in all the subdomains, especially in the Mesorif (Fig. 7). During late Serravallian–early Tortonian, distality increases in the Internal Intrarif and decreases during middle–late Tortonian in the External Prerif. Additionally, the Ill(002):Ill(001) ratios ≥0.40 and the lower abundance of smectite (Fig. 7) could suggest some weak burial diagenesis associated to second-order syn-sedimentary tectonic events (Nieto et al., 1996; Lanson et al., 2009; Moiroud et al., 2012). The more evident ones are observed during Aquitanian in the Internal Intrarif, Burdigalian in the Mesorif, Langhian in the Internal Prerif, late Serravallian–early Tortonian in the Internal Intrarif, and middle Tortonian in the External Prerif. This source-area history suggests a complex erosional evolution

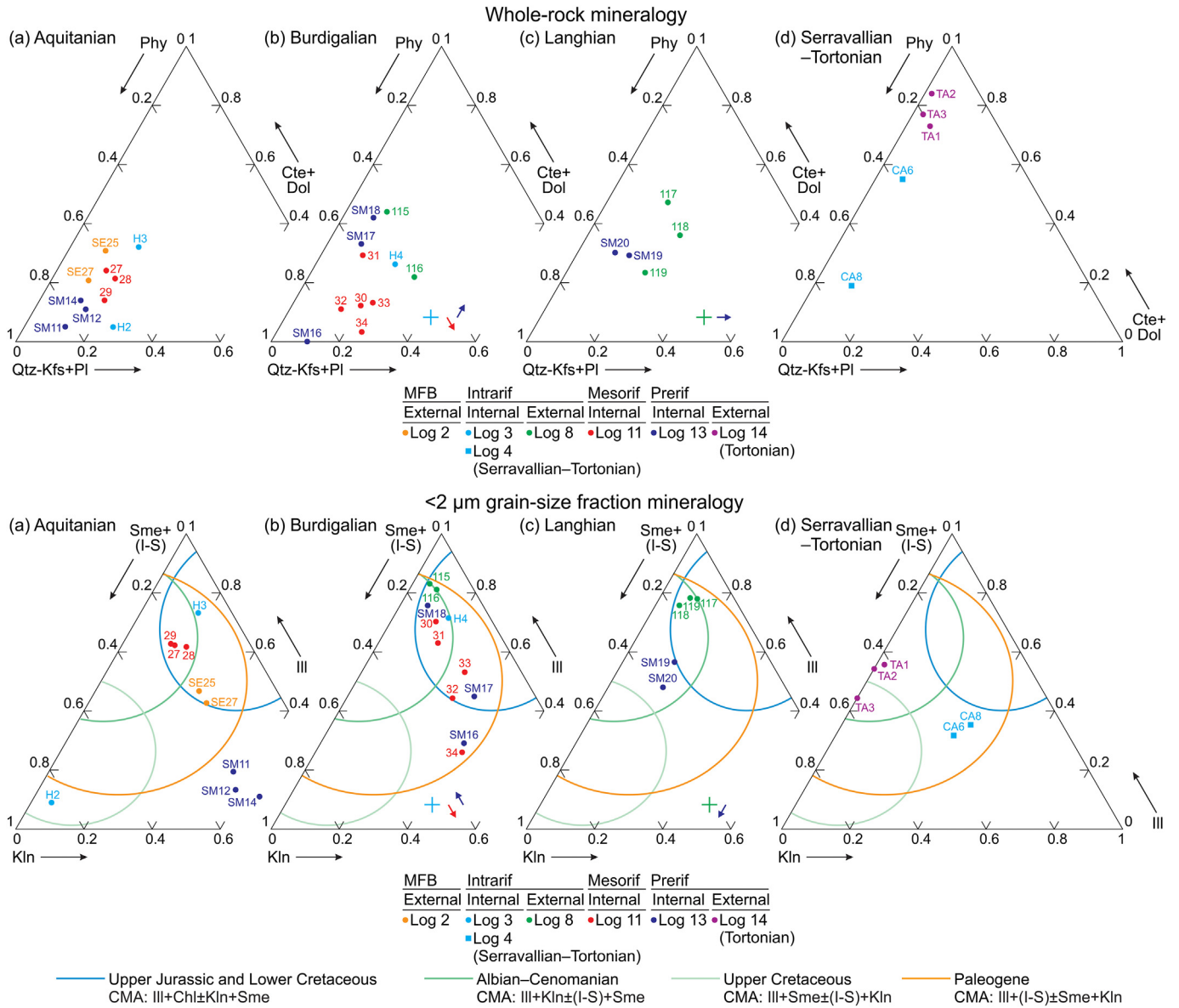


**Fig. 11.** Ternary plots showing the whole-rock and clay-fraction mineralogical associations of studied mudstones from Log 2 (Seguedla) in the Numidian Unit (External MFB), Log 3 (Saf Haman) and Log 4 (Charf El Akab) in the Tanger Unit (Internal Intrarif Subdomain), Log 8 (Douar Ahel Chane) in the Ouezzane Unit (External Intrarif Subdomain), Log 11 (Fej El Hanout) in the Zoumi Unit (Mesorif Subdomain), Log 13 (Sidi M'rabit) in the Larache Unit (Internal Prerif Subdomain), and Log 14 (Talaghaza) in the Ridges Unit (External Prerif Subdomain). Data are clustered by ages of sequences in each log as (A) Aquitanian, (B) Burdigalian, (C) Langhian, and (D) Serravallian–Tortonian. Location of samples and sample label displayed over data points as in Fig. 2. The clay-mineral association (CMA) fields documented in the literature for Upper Jurassic and Lower Cretaceous, Albian–Cenomanian, Upper Cretaceous, and Paleogene External Rifian formations are indicated to infer the source areas evolution. Qtz—quartz; Phy—phyllosilicates; Cte—calcite; Dol—dolomite; Kfs—K-feldspar; Pl—plagioclase; Sme—smectite; III—illite; I-S—random mixed layer illite-smectite; Kln—kaolinite. In plots (B) and (C), arrows show the evolution of the mineral association of the plotted succession in relation to the previous plotted succession (Supplementary Material A5).

in the whole area. The absence of a clear unroofing trend very probably determines supplies resulting from the above discussed mixing of deposits from different rocks and ages.

##### 6.5. Thickness analysis and proposition of the depozones

Although no corrections are made for sediment compaction, nor typical parameters-values nor subsidence curves have been used, an analysis of thicknesses of measured sections has been performed. This approach allows a realistic scalable comparison among different sectors with the hypothetical reconstruction of the main depozones of the margin (De Celles and Giles, 1996: subsiding and rising areas as bulges) and the possible basement tectonic motions in the western ERZ (Fig. 12). For

these considerations, the External MFB stratigraphic sections (Logs 1 and 2) were understood as minimum thicknesses since tectonically laminated (Abbassi et al., 2021, 2022). This evaluation was carried out for the entire Miocene succession and also separately for the Burdigalian (which in our opinion is the best represented, less affected by the period of tectonic lamination and/or erosion throughout the area), Langhian, and Upper Miocene.

##### 6.5.1. Paleogene thicknesses (Martín-Martín et al., 2023)

During the Paleocene–Eocene, the depocenter (foredeep area) was located in the Mesorif–Internal Prerif area, while the forebulge should be located in the External Prerif (Ridges Unit). During the Oligocene, a homogenization of thicknesses took place in the whole basin.

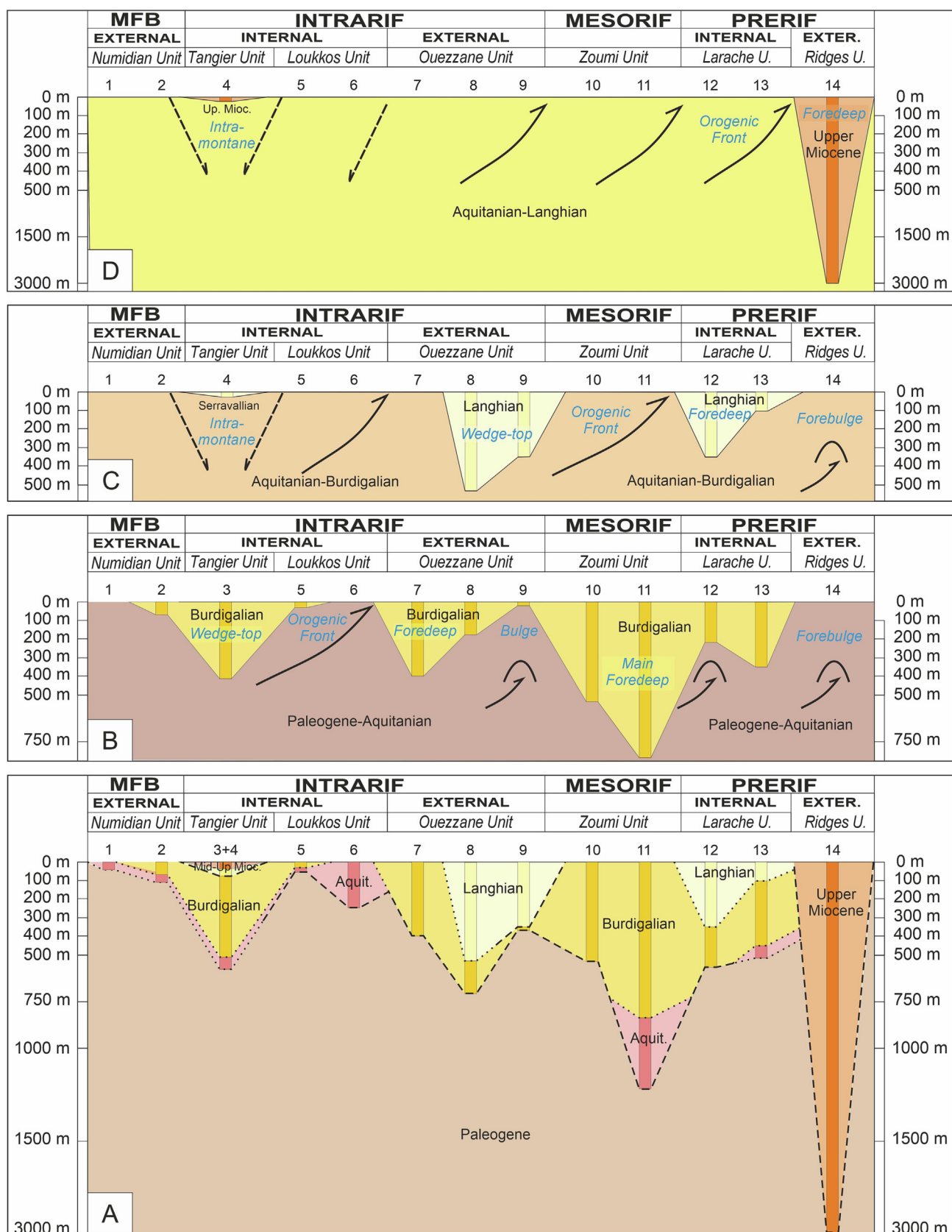


Fig. 12. Thickness analyses of the External Rif Zone. (A) Miocene thicknesses. (B) Burdigalian thicknesses. (C) Langhian thicknesses. (D) Upper Miocene thicknesses.

### 6.5.2. Total Miocene thicknesses

After the Oligocene homogenization of thickness, the Miocene shows again diversification of depocenters (Fig. 12A). The higher thicknesses (>3000 m: main foredeep) are measured in the “Prerifian Ridge” Unit (Log 14), followed by the Mesorif (>1000 m in the Zoumi Unit: Log 11). Other areas with high thicknesses are the External Intrarif (~750 m in the Ouezzane Unit: Log 8) and the Internal Prerif (>500 m in the Larache Unit: Log 13).

### 6.5.3. Burdigalian thicknesses (Fig. 12B)

The thicknesses of the External MFB (Logs 1 and 2) are very probably underestimated for tectonic lamination but we can suppose a very high thickness related to a deep basin realm (Abbassi et al., 2021, 2022). Therefore, the greatest measured thicknesses in the North-African Margin are located in the Mesorifian Zoumi Unit (~750 m in Log 11 and ~500 m in Log 10) which can be considered as a foredeep (Ben Yaich et al., 1989). A similar thickness (300–400 m) is found in Larache Unit (Internal Prerif), Ouezzane Unit (External Intrarif) and Tangier Unit (Internal Intrarif). In this period, the rising areas (forebulges) were located in the Loukkos Unit (Internal Intrarif), external most part of the Ouezzane Unit (External Intrarif) and “Prerifian Ridge” Unit (External Prerif). Since the Burdigalian sedimentation (with variant thicknesses) is recorded in all logs from Ouezzane to Larache units (from External Intrarif to Internal Prerif), the entire area should be considered as a foredeep complex with minor internal bulges probably related to fault-propagation folds (blind thrusts) (Zakir et al., 2004). In this case, the main foredeep area would be located in the Mesorif (Zoumi Unit, Log 11). The recorded sedimentation in the Tangier and Loukkos Units (Internal Prerif) – disconnected from the complex foredeep – could be considered as a wedge-top area related to the orogenic front which should be located in the Loukkos and Ouezzane Units boundary (the Internal–External Intrarif boundary). In this context, the Prerifian “Prerifian Ridge” Unit without sedimentation in this period could be considered as a forebulge due also probably to a fault-propagation fold system.

### 6.5.4. Middle and Upper Miocene thicknesses

The sedimentation during this period is much lesser and discontinuous in time and space along the North-African Margin (Fig. 12A). Moreover, in many cases, the top of the sedimentation corresponds with the erosive topographic surface of today (Abbassi et al., 2020) and the results obtained here must be taken with due caution. During the Middle Miocene, the sedimentation is limited to the Langhian (Fig. 12C) with thicknesses of ~500 m (Log 8) in the Ouezzane Unit (External Intrarif) and ~300 m (Log 12) in the Larache Unit (Internal Prerif). During the Middle Miocene, the foredeep probably migrated south-westward from the Mesorif to the Internal Prerif and was limited to the Larache Unit area. The structuring of the ERZ progressed and thrusts move south-westward. The other sedimentary area in the Ouezzane Unit (External Intrarif) probably constituted a new wedge-top area considering the new position of the orogenic front roughly in the Mesorif. The Prerifian Ridges Unit that remains still without sedimentation until this period (Martín-Martín et al., 2023) would continue to act as the forebulge due to the fault-propagation fold (Martín-Martín et al., 2001). During the Upper Miocene, the sedimentation is reduced to two opposite areas (Fig. 12D), with thickness ~3000 m in the “Prerifian Ridge” Unit (External Prerif) and ~100 m in the Tangier Unit (Internal Intrarif). During this phase, probably the foredeep migrated again south-westward to the “Prerifian Ridge” Unit of the External Prerif (former forebulge). The orogenic front would be located in this period in the Internal–External Prerif boundary. Sedimentation is recorded again in the Tangier Unit (Internal Intrarif) probably in this case in postorogenic conditions as an intramontane basin.

### 7. Miocene 2D paleogeographic-paleotectonic modeling

The previously described multidisciplinary approach led to a tentative 2D evolutionary model (maps and cross-sections) of the ERZ during the Miocene in its regional context. This result was achieved using GPlates basemaps according to Müller et al. (2018, 2019) and Le Breton et al. (2021). In Fig. 13 Europe is always considered the fixed plate. Fig. 13A shows a general paleogeographic and paleotectonic reconstruction in the western Tethys during the late Cretaceous after a long extensional phase (Guerrera et al., 2021). Some authors propose a plate tectonic evolution for the area with a unique oceanic branch corresponding with the MFB in a progressive deformation affecting the Paleogene and Miocene subduction below a continental domain called AlKaPeCa (Faccenna et al., 2001; Schettino and Turco, 2011; Carminati et al., 2012; Lustrino et al., 2013; Rossetti et al., 2013; Leprêtre et al., 2018). But, in our opinion two oceanic branches are necessary to explain the central-western Mediterranean geology (Doglioni, 1992; Guerrera et al., 2021; Martín-Martín et al., 2023; among others). Between the MM and the European margins (here considered the closer South Iberian Margin) an oceanic space (corresponding with the Nevado–Filabride–Liguride–Piemontese Units) closed with plate collisions with northward vergence during the Paleogene giving rise to the Eo-alpine system. This evolution, if took place as we believe (Guerrera et al., 2021; cum bibl.) did not affect the North African Margin studied in this work. Therefore, the modellization of the evolution of the North African Margin is independent of the general model preferred (MM vs AlKaPeCa). There is consensus in the idea of the MFB oceanic branch separating the North Africa Margin and the plate (MM) or domain (AlKaPeCa) origin of the Internal Rif Zones (Faccenna et al., 2001; Schettino and Turco, 2011; Carminati et al., 2012; Doglioni, 1992; Lustrino et al., 2013; Rossetti et al., 2013; Leprêtre et al., 2018; Guerrera et al., 2021; Martín-Martín et al., 2023; among many others). There is substantial agreement in that the closure of this last oceanic branch and derived plate collisions should give rise to the structuring of the Rif Chain and by extension to the neo-Alpine Maghrebian system: Betic, Rif-Tell and Apennine chains (Guerrera et al., 2021). Furthermore, the North Africa Margin recent papers supported the existence of minor lateral basinal branches characterized by oceanic-transitional crust as in the case of the External Intrarif area (Benzaggagh, 2016; Benzaggagh et al., 2013). As before commented, for the ERZ all published alpine models are substantially in good agreement considering at the beginning of the latest Cretaceous the tectonic inversion from extensional to compressional in the Tethyan domains (Stampfli et al., 2002). During the Paleogene, the Eo-alpine compressional phase (Alpine s.s.) developed creating the alpine European chains as Pyrenees, Iberian range of the Alps (Martín-Martín et al., 2001; Faccenna et al., 2001; Schettino and Turco, 2011; Carminati et al., 2012; Doglioni, 1992; Lustrino et al., 2013; Rossetti et al., 2013; Leprêtre et al., 2018; Guerrera et al., 2021). The Paleogene evolution (marked by compressional axis W–E oriented) of the NW Africa margin is deeply treated in a previous work to which it refers (Martín-Martín et al., 2023).

During the Miocene convergence (Fig. 13B to D), the compressional axis rotates from W–E to close N–S acting the External Rif Zone as a complex foreland system (Abbassi et al., 2020). More in detail, during the early Miocene (Fig. 13B) the opening of the Mediterranean area accounted as a back-arc basin while the extension took place in the Internal Zone constituted by the MM (Guerrera et al., 2021). As a result, in the ERZ compression, shortening and subductions of the MFB together with the External Intrarif brach occurred (Martín-Martín et al., 2023). During the early Miocene the main sedimentary depozones represented the Internal Intrarif, External Intrarif and Internal Mesorif (foredeep) while the orogenic front was located in the Internal–External Intrarif boundary. During the middle Miocene (Fig. 13C) we assume that both subductions are sutured and units from these domains now are floating

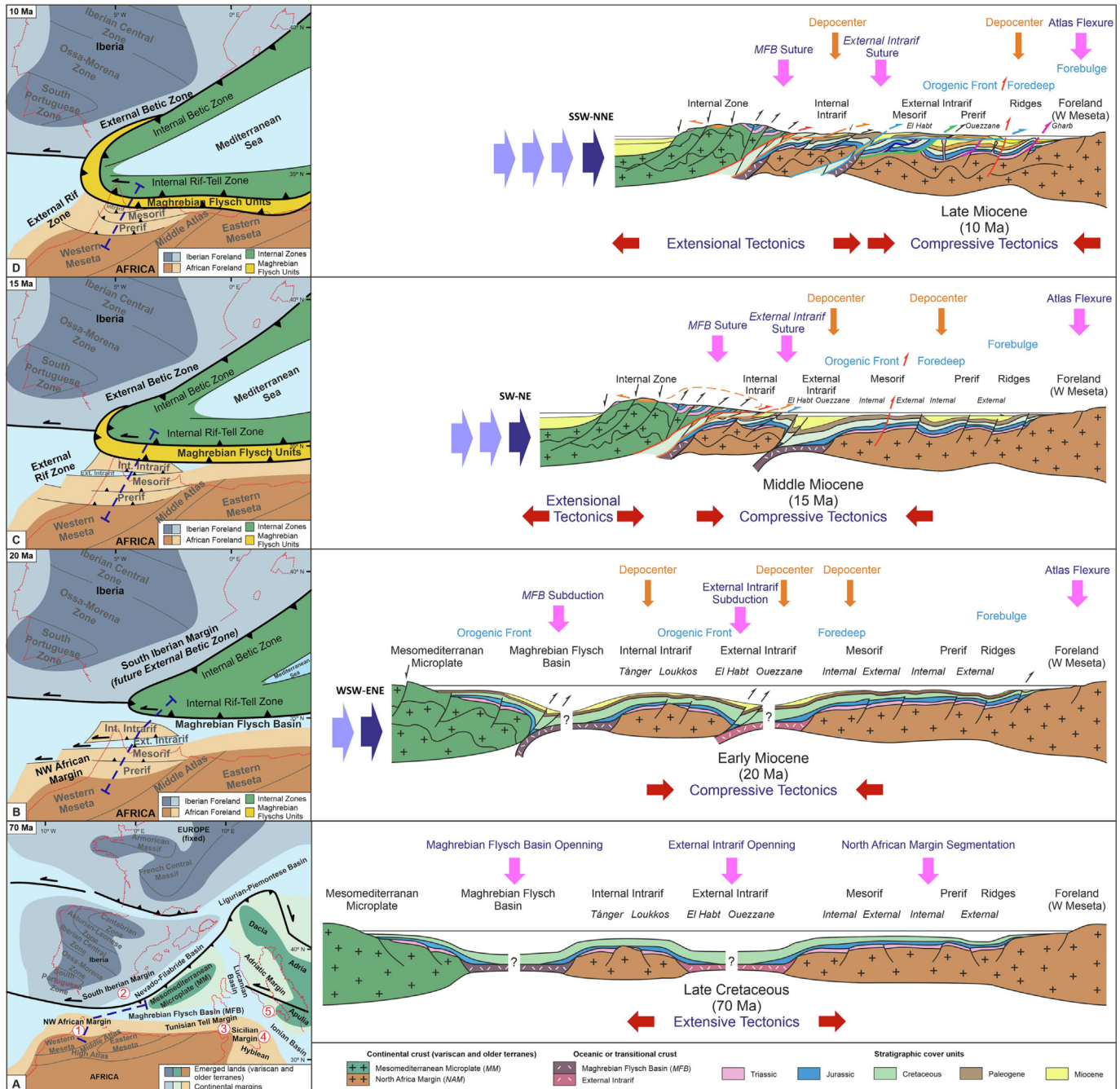


**Fig. 13.** Paleogeographic-geodynamic models based on GPlates maps after Müller et al. (2019) and Le Breton et al. (2021). (A) Paleogeographic-geodynamic map of the western-central Mediterranean area at the late Cretaceous times; the five sectors compared in Fig. 14 are indicated. (B) Paleogeographic-geodynamic detailed map of the External Rif Zone area at the lower Miocene times. (C) Paleogeographic-geodynamic detailed map of the External Rif Zone area at the middle Miocene times. (D) Detailed paleogeographic-geodynamic cross-sections of the External Rif Zone area with evidenced the crustal basement, and emphasizing the stratigraphic cover units at the late Cretaceous, lower Miocene and middle Miocene.

and unrooted extruded units. The Internal Zone becomes a back-arc extension while the ERZ followed in compression (Guerrera et al., 2021). The convergence axis rotated to SW-NE (Abbassi et al., 2020); the orogenic front is now located in the Mesorif and the main depositional areas become the External Infratirif as a wedge-top basin and the Internal Prerif as the foredeep. Finally, during the late Miocene (Fig. 13D) the nappe structuring of the External Rif Zone was marked by SSW-NNE convergence axis (Abbassi et al., 2020). In this last period, the orogenic front migrates to the Prerif while the foredeep basin was located in the Ridges area. In the Infratirif zone postorogenic intramontane basins appeared.

## 8. Comparison with other central-western Tethyan margins

### 8.1. South Iberian Margin

This margin (Vera, 2004) is represented along the External Betic Cordillera (South Spain) as part of the alpine margin of the westernmost Tethys (sector 2, Fig. 13A). The Betic sector (Fig. 14) is distinguished into two main complexes: Subbetic and Prebetic tectonically overlapping (Fig. 14). The structuring of this margin took place progressively from internal to external with a NW direction during the Miocene starting in Middle Miocene in southern sectors and ending in the Late Miocene

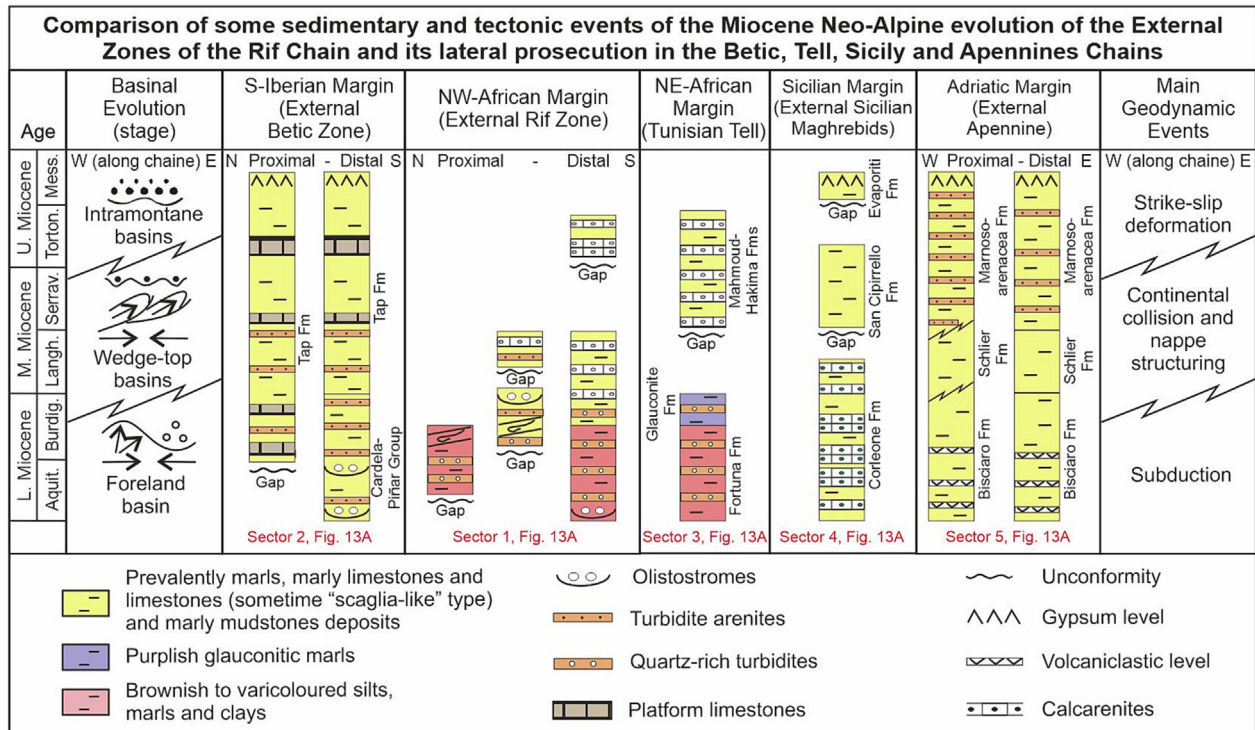


**Fig. 14.** Correlation of the stratigraphic chart and basinal evolution stages of the Rif Chain (sector 1 in Fig. 13A) to the reported ones in other Tethyan margins (sectors located in Fig. 13A) of the same orogenic system, as South Iberian Margin (sector 2 in Fig. 13A), Tunisian Tell (sector 3 in Fig. 13A), Sicilian Margin (sector 4 in Fig. 13A), and Adriatic Margin (sector 5 in Fig. 13A).

in the northern ones (Vera, 2000). During the Miocene both domains evolved as a foreland basin (Vera, 2000; Guerrera et al., 2006, 2014) characterized by a diversification of lithofacies within local marine deep basins located between rising emergent areas. In lower Miocene the deep Subbetic areas scaglia-like lithofacies deposited (Cardela Group) with frequent olistostromes (Píñar Group) near the emergent reliefs. On the contrary, in the Prebetic Domain, a shallow calcareous platform developed. The middle Miocene sedimentation shows a certain homogenization of deep marine lithofacies and siliceous marls deposits (Tap Fm or Albarizas facies) (Vera, 2000; Guerrera et al., 2006, 2014). The upper Miocene sedimentation is restricted to the Guadalquivir Foreland Basin characterized by olistostromic deposits, but also by intramontane post-orogenic basins where calcarenites (shallow marine) and marls (deep marine) are common in the Subbetic (Vera, 2000). More in general, the upper Miocene sedimentation shows a regressive trend with Messinian gypsum deposits. Nappe tectonic took place in the Subbetic during the middle Miocene, later in the Prebetic, during the upper Miocene (Vera, 2000). This tectono-sedimentary evolution shows significant similarities with the ERZ, in terms of kind of deposits, timing of structuring and paleogeography. Nevertheless, as counterpart the vergence of structuring is in opposite direction.

## 8.2. Tunisian Tell Margin

Also, this sector shows a wide alpine margin where four main zones are currently recognized (Rouvier, 1977, 1985; Van Houten, 1980; Wildi, 1983; Belayouni et al., 2010, 2012, 2023b; Martín-Martín et al., 2023). They are characterized by different tectonic units showing a southern vergence (sector 3, Fig. 13A): (1) Numidian Zone; (2) Triassic Dome Zone; (3) Intermediate Atlas Zone; and (4) Saharan Zone. During the Early Miocene, while Numidian successions deposited in MFB, different lateral formations, gradually younger toward more external areas, generated on the Tunisian Margin, sometimes associating atypical Numidian lithofacies (Fig. 14). The shallow marine suites: Fortuna-Salambo Fms (Oligocene-Early Miocene), Glauconite Fm (upper

Burdigalian) and Hakima-Mahmoud Fms (Middle-Late Miocene) represent the sedimentation in the whole margin area (Belayouni et al., 2013, 2023a, 2023b). In addition, these last formations are equivalent to the Abarizas-Moronitas facies in the South Iberian Margin. The upper Miocene sedimentation also shows a regressive trend with Messinian gypsum deposits (Rouvier, 1977, 1985). This Tunisian margin also shows a similar deformative evolution with respect to the previous South Iberian and the NW African ones with a progressive southward oriented nappe evolution from Internal to External during the Middle-Late Miocene.

## 8.3. Sicilian Margin

The SE-vergent External Zones of the Sicilian Maghrebids, show a paleogeographic and paleotectonic evolution similar to the other margins previously described (sector 4, Fig. 13A). The main paleogeographic external Sicilian pre-Miocene domains result: (1) the Panormide carbonate platform, and (2) the deep-water Imerese Basin that pass toward east to sectors bordered by shallow water and pelagic platforms (Trapanese and Saccense) and Iblean Foreland (SE Sicily). The most accepted regional reconstruction indicates that the Imerese units override the Panormide ones (Catalano et al., 1993, 1996, 2013; Casero and Roure, 1994; Giunta et al., 2000; Gasparo Morticelli et al., 2015; among others). Nevertheless, other authors have more recently proposed different reconstructions (Finetti, 2005; Basilone, 2009, 2018; Lentini and Carbone, 2014; Henriet et al., 2020; and references therein). The Miocene sedimentation of the external zones shows lateral variation and the lithofacies associations indicate different depositional environments. During the Miocene two main successions characterize the sedimentation the Sicanian and Trapanese domains (Fig. 14): (i) the prevalently glauconitic calcarenites (Corleone Calcarenites Fm, Aquitanian-Langhian); (ii) pelagic marls and marly clays (San Cipirrello Fm, Serravallian-lower Tortonian) respectively (Henriet et al., 2020). Both these formations are part of the external thrust system linked to the deformed margin of the Africa-Adria plates

(Lentini and Carbone, 2014). The occurrence of syn-sedimentary faults and folds at different stratigraphic levels of the Paleogene and Miocene foredeep successions and relative deformations (Gasparo Morticelli et al., 2015; and references therein) completes the similarity with the external sectors previously considered. Regarding stratigraphic gaps of the Miocene foredeep and related unconformities checked in the stratigraphic record of the Rif (Morocco) (see above), and those identified in other lateral chains it is not easy to establish some correlations for the diversity of the successions.

#### 8.4. Adriatic Margin

The E-vergent External Zones of the Apennines can be schematically represented by two main domains located south and north of the Ancona-Anzio tectonic line respectively: (1) the Campania-Lucania and the southern Lazio-Abruzzi sectors; and, (ii) the more external Umbria-Marche Domain belonging to the Adria Margin progressively emplaced eastward. Even if these areas show some paleogeographic peculiarities, the general evolution is comparable with the previously considered chains of the South Iberian and African margins (sector 5, Fig. 13A). The Lazio-Abruzzi, Campania-Lucania and Umbria-Marche units are represented by sedimentary successions deposited on the Hercynian continental crust of the Adria-Africa Margin, dismembered and drifting northward during the Cenozoic to reach the present position (Fig. 14). In the Umbria-Marche sector the Lower Miocene is characterized by marls, marly limestones with interbedded volcaniclastic beds (Bisciaro Fm) constituting a very representative regional marker (Guerrera et al., 2015). After a Middle Miocene marly episode very rich in microfossils of open sea and very reduced clastic supply (Schlier Fm) the sedimentation becomes terrigenous: marls and turbiditic arenites (Marnoso-arenacea Fm). This last external formation is very thick, extensive and diachronic ranging the base of the Messinian. This last sedimentary evolution attests an upward increasing of the tectonic activity. Similar Miocene lithological suites and syn-sedimentary structures are also recognizable in the Lazio-Abruzzi and Campania-Lucania domains but the volcaniclastic supply is rare (Vitali et al., 2017). More details are in Martín-Martín et al. (2023).

### 9. Conclusions

- 1- The Miocene evolution of the External Rif (Morocco) and its comparison with similar Mediterranean Tethyan margins is proposed.
- 2- Three depositional sequences are reconstructed as Aquitanian-Burdigalian, Langhian, and Tortonian-Messinian separated by three unconformities with associated stratigraphic gaps across (1) Oligocene–Miocene boundary (gap: upper Oligocene–lower Burdigalian); (2) Burdigalian–Langhian boundary with local widespread in the Ouezzane Unit (gap: upper Burdigalian); (3) Middle–Upper Miocene boundary (gap: mostly upper Langhian–lowermost Tortonian, the whole pre-Tortonian Miocene being found in the Ridges Unit).
- 3- The unconformities are coincident in time with regional deformation phases affecting the western Tethys as (1) pre-Miocene structuring of the Internal Zone; (2) flexural deformation of the Atlas front across the Oligocene–Miocene boundary; (3) diachronic closure of the MFB; (4) extrusion of the MFB deposits (flyschs nappes) starting from the Middle Miocene; and (5) nappes propagation southward toward the ERZ during the Middle–Late Miocene times.
- 4- The sedimentary record shows a wide variety of lithofacies associations linked to the diversification of sedimentation environments that passed from a carbonate platform to a deep basin. These deposits show indicators of synsedimentary tectonics identified by mass flow deposits (tectofacies), synsedimentary faults, development of unconformities, petrographical and mineralogical suites,

as well as the variable thicknesses among the formations. The conjunction of all these elements reinforces the idea of a syn-sedimentary tectonics affecting the margin/basin system during the Miocene.

- 5- The petrographic results suggest a middle- to high-grade metamorphic source in a variable context from an Interior Craton to Quartzose-Transitional Recycled orogen. The Atlas Chain and the African Craton are here proposed for this metamorphic source area.
- 6- The mineralogical results suggest mixture of sediments coming from the erosion of Upper Jurassic to Paleogene suites, especially from kaolinite-rich Albian–Cenomanian to smectite-rich Paleogene, with absence of a clear unroofing. Provenance analysis indicated local and distal source areas probably from active tectonic areas in uplifting.
- 7- The thickness analysis of the studied sedimentary successions allows proposing the evolution of the orogenic front and main depozones (foredeep, bulges, wedge-top and intramontane sub-basins) integrated in a complex foreland system migrating from north to south in three phases: Early, Middle and Late Miocene. The orogenic front moved from the Internal Intrarif to Mesorif and to Internal Prerif in these phases. The main wedge-top basin also migrated from the Internal Intrarif to External Intrarif. The foredeep evolved from the Mesorif to the Internal Prerif, while the main forebulge was located in the External Prerif and a secondary bulge developed in the External Intrarif. Intramontane basins developed behind the orogenic front in relative extensional conditions moving from the Internal Extrarif to External Intrarif.
- 8- A 2D evolutionary model using GPlates reconstructions as basemap is proposed on the basis of an oceanic area (Maghrebian Ocean) located between the Mesomediterranean Microplate (to the north) and the North Africa Margin (to the south). During the Miocene the tectonic convergence was contemporaneous with axis rotation from W–E to close N–S. In this phase the External Rif Zone acted as a complex foreland system with an internal oceanic branch in the External Intrarif Domain.
- 9- The reconstructed tectonic-sedimentary evolution is compared to that reported in other margins of the central-western peri-Mediterranean chains (S-Iberian, Tunisian Tell, Sicily's chains and Apennine). Considering some local differences in the timing of processes (as an evident diachronism between W–E and N–S branches of the considered chains attests), a geodynamic evolution including convergence-continental collision-nappe structuring-strike slip deformation is found. More or less complex foreland basins evolve into wedge top and intramontane basins. In particular and in all cases, mass flow deposits (turbidites, slumps, olistostromes) are very abundant. In addition, similar unconformities checked in the Rif have been registered in the African-Sicilian margins while more continuous sedimentation is registered in the S-Iberian and Adriatic margins. A significant volcaniclastic supply took place in the eastern sectors (mainly in Sicily and southern Apennines) during the early Miocene.

Supplementary data to this article can be found online at <https://doi.org/10.1016/j.sedgeo.2024.106619>.

#### CRediT authorship contribution statement

**Manuel Martín-Martín:** Conceptualization, Data curation, Formal analysis, Funding acquisition, Investigation, Methodology, Writing – original draft, Writing – review & editing. **Francesco Guerrera:** Investigation, Writing – original draft, Writing – review & editing. **Juan Carlos Cañaveras:** Investigation, Writing – original draft, Writing – review & editing. **Francisco Javier Alcalá:** Investigation, Writing – original draft, Writing – review & editing. **Francisco Serrano:** Investigation, Writing – original draft, Writing – review & editing. **Alí Maaté:** Investigation. **Rachid Hlila:** Methodology, Writing – original draft. **Soufian Maaté:**

**Investigation. Antonio Sánchez-Nava:** Investigation. **Crina Miclăus:** Investigation. **José Enrique Tent-Manclús:** Investigation. **Manuel Bullejos:** Investigation, Software.

## Data availability

Data will be made available on request.

## Declaration of competing interest

The authors declare no conflict of interest.

## Acknowledgments

Research supported by PID2020-114381GB-I00 Research Project (Spanish Ministry of Education and Science), EU HORIZON project CiROCCO under Grant Agreement No 101086497, Research Groups and projects of the Generalitat Valenciana from Alicante University (CTMA-IGA), and Research Group RNM-188 of the Junta de Andalucía from EEZA-CSIC. The help from Eline Le Breton from the Freie Universität (Berlin, Germany) with the GPlates base map is greatly acknowledged.

## References

- Abbassi, A., Cipollari, P., Zaghlool, M.N., Cosentino, D., 2020. The Rif Chain (Northern Morocco) in the Late Tortonian-Early Messinian Tectonics of the Western Mediterranean Orogenic Belt: evidence from the Tangier-Al Manzla Wedge-Top Basint. *Tectonics* 39, https://doi.org/10.1029/2020TC006164.
- Abbassi, A., Cipollari, P., Zaghlool, M.N., Cosentino, D., 2021. The Numidian Sandstones in northern Morocco: evidence for early Burdigalian autochthonous deposition on top of the Tanger Unit. *Marine and Petroleum Geology* https://doi.org/10.1016/j.marpetgeo.2021.105149.
- Abbassi, A., Cipollari, P., Fellini, M.G., Zaghlool, M.N., Guillong, M., El Mourabet, M., Cosentino, D., 2022. The Numidian sand event in the Burdigalian foreland basin system of the Rif, Morocco, in a source-to-sink perspective. *The Geological Society of America Bulletin* 134 (9–10), 2280–2304.
- Abdelmalek, B., Rekia, B., Youcef, B., Lakhdar, B., Nathalie, F., 2017. Mineralogical characterization of Neogene clay areas from the Jijel basin for ceramic purposes (NE Algeria-Africa). *Applied Clay Science* 136, 176–183.
- AitBrahim, L., Chotin, p., Hinaj, S., Abdellouafi, A., El Adraoui, A., Nakcha, Ch., Dhont, D., Charroud, M., SosseyAlaoui, F., Amrhar, M., Bouaza, A., Tabyaoui, H., Chaouni, A., 2002. Paleostress evolution in the Moroccan African margin from Triassic to present. *Tectonophysics* 357, 187–205.
- Alcalá, F.J., Martín-Martín, M., López-Galindo, A., 2001. Clay mineralogy of the Tertiary sediments in the Internal Subbetic of Málaga Province, Spain: implications for geo-dynamic evolution. *Clay Minerals* 36, 615–620.
- Alcalá, F.J., López-Galindo, A., Martín-Martín, M., 2013a. Clay mineralogy as a tool for integrated sequence stratigraphic and palaeogeographic reconstructions: Late Oligocene-Early Aquitanian Western Internal South Iberian Margin, Spain. *Geological Journal* 48, 363–375.
- Alcalá, F.J., Guerrera, F., Martín-Martín, M., Raffaelli, G., Serrano, F., 2013b. Geodynamic implications derived from Numidian-like distal turbidites deposited along the Internal-External Domain Boundary of the Betic Cordillera (Spain). *Terra Nova* 25, 119–129.
- Asebriy, L., de Luca, P., Bourgois, J., Chotin, P., 1987. Resédimentation d'âge sénonien dans le Rif central (Maroc): conséquences sur les divisions paléogéographiques et structurales de la chaîne. *Journal of African Earth Sciences* 6, 917.
- Asebriy, L., Azdimousa, A., Bourgois, J., 2003. Structure du Rif externe sur la transversale du Massif de Ketama. *Travaux de l'Institut Scientifique, Rabat, Maroc* 21 pp. 27–46.
- Azdimousa, A., Bourgois, J., Asebriy, L., Poupeau, G., Montigny, R., 2003. Histoire thermique et surrection du Rif externe et des nappes de flyschs associées (Nord Maroc). *Travaux Institut Scientif. Univ. Mohammed V. Série Géologie et Géographie Physique* 21 pp. 15–26.
- Azdimousa, A., Jabaloy, A., Asebriy, L., Booth-Rea, G., González-Lodeiro, F., Bourgois, J., 2007. Lithostratigraphy and structure of the Temsamane Unit (Eastern External Rif, Morocco). *Revista de la Sociedad Geológica de España* 20, 119–132.
- Bargach, K., Ruano, P., Chabli, A., Galindo-Zaldívar, J., Chalouan, A., Jabaloy, A., Akil, M., Ahmamou, M., Sanz de Galdeano, C., Benmakhlouf, M., 2004. Recent tectonic deformations and stresses in the frontal part of the Rif Cordillera and the Saïss Basin (Fes and Rabat regions, Morocco). *Pure and Applied Geophysics* 161, 521–540.
- Basilone, L., 2009. Sequence stratigraphy of a Mesozoic carbonate platform-to-basin system in Western Sicily. *Central European Journal of Geosciences* 1 (3), 251–273.
- Basilone, L., 2018. *Lithostratigraphy of Sicily*. Springer, Heidelberg, pp. 1–349.
- Basu, A., Young, S.W., Suttner, L.J., James, C.W., Mack, G.H., 1975. Re-evaluation of the use of undulatory extinction and polycrystallinity in detrital quartz provenance interpretation. *Journal of Sedimentary Petrology* 45, 873–882.
- Belayouni, H., Brunelli, D., Clocchiatti, R., Di Staso, A., El Amrani El Hassan, Iz-E., Guerrera, F., Kassaa, S., Laridihi Ouaza, N., Martín-Martín, M., Serrano, F., Tramontana, M., 2010. La Galite Archipelago (Tunisia, North Africa): stratigraphic and petrographic revision and insights for geodynamic evolution of the Maghrebian Chain. *Journal of African Earth Sciences* 56, 15–28.
- Belayouni, H., Guerrera, F., Martín-Martín, M., Francisco Serrano, F., 2012. Stratigraphic update of the Cenozoic Sub-Numidian formations of the Tunisian Tell (North Africa): tectonic/sedimentary evolution and correlations along the Maghrebian Chain. *Journal of African Earth Sciences* 64, 48–64.
- Belayouni, H., Guerrera, F., Martín-Martín, M., Serrano, F., 2013. Paleogeographic and geodynamic Miocene evolution of the Tunisian Tell (Numidian and Post-Numidian Successions): bearing with the Maghrebian Chain. *International Journal of Earth Sciences* 102, 831–855. https://doi.org/10.1007/s00531-012-0824-x.
- Belayouni, H., Guerrera, F., Martín-Martín, M., Le Breton, E., Tramontana, M., 2023a. The Numidian formation and its Lateral Successions (Central-Western Mediterranean): a review. *International Geology Review* https://doi.org/10.1080/00206814.2023.2199429.
- Belayouni, H., Guerrera, F., Martín-Martín, M., Tramontana, M., Bullejos, M., 2023b. Cenozoic tectono-sedimentary evolution of the onshore-offshore Tunisian Tell: implications for oil-gas research. *Marine and Petroleum Geology* 156, 106426. https://doi.org/10.1016/j.marpetgeo.2023.106426.
- Ben Yaich, A., Duee, G., Souquet, P. et, Fondecavallez, j.M., 1989. Les grès de Zoumi: dépôts turbiditiques d'une Avant-fosse moclène (Burdigalien-Serravallien) dans le Rif occidental (Maroc). *C.R. Acad. Sc., Paris* 309, série II pp. 1819–1825.
- Benzagagh, M., 2016. Tholeitic basalts and ophiolitic complexes of the Mesorif Zone (External Rif, Morocco) at the Jurassic-Cretaceous boundary and the importance of the Ouerrah Accident in the palaeogeographic and geodynamic evolution of the Rif Mountains. *Boletín Geológico y Minero* 127, 389–406.
- Benzagagh, M., Mokhtari, A., Rossi, Ph., Michard, A., El Maz, A., Chaouan, A., Saddiqi, O., Rjimati, E.-C., 2013. Oceanic units in the core of the External Rif (Morocco): intramargin hiatus or South-Tethyan remnants. *Journal of Geodynamics* 77, 4–21.
- Berggren, W.A., Pearson, P.N., 2006. Tropical and subtropical planktonic foraminiferal zonation of the Eocene and Oligocene. In: Pearson, P.N., Olsson, R.K., Huber, B.T., Hemleben, C., Berggren, W.A. (Eds.), *Atlas of Eocene Planktonic Foraminifera*. Cushman Foundation Special Publication vol. 41. Alen Press, Lawrence (Kansas, USA), pp. 29–40.
- Berggren, W.A., Pearson, P.P., 2005. A revised tropical to subtropical planktonic foraminiferal zonation of the Eocene and Oligocene. *Journal of Foraminiferal Research* 35, 279–298.
- Biscaye, P.E., 1965. Mineralogy and sedimentation of recent deep-sea clay in the Atlantic Ocean and adjacent seas and oceans. *Geological Society of America Bulletin* 76, 803–832.
- Blow, W.H., 1969. Late middle Eocene to recent planktonic foraminiferal biostratigraphy. In: Brönniman, P., Renz, H.H. (Eds.), *Proceedings of the 1st International Conference on Planktonic Microfossils*. Geneva (Swiss) vol. 19671, pp. 199–422.
- Boukaoud, E.H., Godard, G., Chabou, M.C., Bouftouha, Y., Doukkari, S., 2021. Petrology and geochemistry of the Texenna ophiolites, northeastern Algeria: implications for the Maghrebian flysch suture zone. *Lithos*, 390–391 https://doi.org/10.1016/j.lithos.2021.1060190024-4937.
- Carminati, E., Lustrino, M., Doglione, C., 2012. Geodynamic evolution of the central and western Mediterranean: tectonics vs. igneous petrology constraints. *Tectonophysics* 579, 173–192.
- Caserio, P., Roure, F., 1994. Neogene deformations at the Sici-lian-North African plate boundary. In: Roure, F. (Ed.), *Peri-Te-Thian Platforms*. Institut Francais du Pétrole Research Conference, Arles, Proceedings. Editions Technip, Paris, pp. 27–50.
- Catalano, R., Di Stefano, E., Lo Cicero, G., Infuso, S., Vail, P.R., Vitale, F.P., 1993. Basin analysis and sequence stratigraphy of the Plio-Pleistocene of Sicily. In: Max, M.D., Colantoni, P. (Eds.), *Geological Development of the Sicilian-Tunisian Platform*. Proceedings of international Scientific Meeting Held at the University of Urbino, Italy, 4–6 November, 1992. Unesco Report in Marine Science58, pp. 99–104.
- Catalano, R., Di Stefano, P., Sulli, A., Vitale, F., 1996. Paleogeography and structure of the Central Mediterranean: Sicily and its offshore area. *Tectonophysics* 260 (4), 291–324.
- Catalano, R., Valentì, V., Albanese, C., Acciaino, F., Sulli, A., Tinivella, U., Gasparo Morticelli, M., Zanolla, C., Giustiniani, M., 2013. Sicily's fold-thrust belt and slab roll-back: the SI. RI. PRO. seismic crustal transect. *Journal of the Geological Society* 170 (3), 451–464.
- Catuneau, O., Galloway, W.E., Kendall, C.G., St, C., Miali, A.D., Posamentier, H.W., Strasser, A., Tucker, M.E., 2011. Sequence stratigraphy: methodology and nomenclature. *Newsletters on Stratigraphy* 44 (3), 173–245.
- Chalouan, A., Galindo-Zaldívar, J., Akil, M., Marín, C., Chabli, A., Ruano, P., Bargach, K., Sanz de Galdeano, C., Benmakhlouf, M., Ahmamou, M., Gourari, L., 2006. Tectonic wedge expulsion in the southwestern front of the Rif Cordillera (Morocco). In: Moratti, G., Chalouan, A. (Eds.), *Tectonics of the Western Mediterranean and North Africa*. Geological Society of London, spec. Publ 262, pp. 101–118.
- Chalouan, A., Michard, A., El Kadiri, K.H., Frizon de Lamotte, D., Soto, J.I., Saddiqi, O., 2008. Continental Evolution: The Geology of Morocco. *Lecture Notes in Earth Sciences* vol. 116. Springer-Verlag, Berlin Heidelberg (Berlin) (424 pp.).
- Chamley, H., 1989. *Clay Sedimentology*. Springer, Berlin (623 pp.).
- Chamley, H., Meulenkamp, J.E., Zachariasse, W.J., Van der Zwaan, G.J., 1986. Middle to Late Miocene marine ecostratigraphy: clay minerals, planktonic foraminifera and stable isotopes. *Oceanologica Acta* 9, 227–238.
- Condie, D.C., 2005. Tectonic settings. Earth as an Evolving Planetary System 3, 59–114. https://doi.org/10.1016/B978-012088392-9/50003-7.
- Critelli, S., 2018. Provenance of Mesozoic to Cenozoic Circum-Mediterranean sandstones in relation to tectonic setting. *Earth-Science Reviews* 185, 624–648.
- Critelli, S., Arribas, J., Le Pera, E., Tortosa, A., Marsaglia, K.M., Latter, K.K., 2003. The recycled orogenic sand provenance from an uplifted belt, Betic Cordillera, Southern Spain. *Journal of Sedimentary Research* 73 (1), 72–81.
- Critelli, S., Muto, F., Perri, F., Tripodi, V., 2017. Interpreting provenance relations from sandstone detrital modes, southern Italy foreland region: stratigraphic record of the Miocene tectonic evolution. *Marine and Petroleum Geology* 87, 2–14.

- Croudace, J.W., Robinson, N.D., 1983. A simple, rapid and precise smear method for the preparation of oriented clay mounts. *Clay Minerals* 18, 337–340.
- Daoudi, L., Deconinck, J.F., Witan, O., Rey, J., 1995. Impact des variations du niveaumarin sur les argiles: exemple du Crétacé inférieur du basin d'Essaouira (Maroc). *Comptes Rendus de l'Académie des Sciences, Paris* 320 pp. 707–711.
- De Celles, P.G., Giles, K.A., 1996. Foreland basin systems. *Basin Research* 8 (2), 105–123.
- Dickinson, W.R., 1970. Interpreting detrital modes of graywacke and arkose. *Journal of Sedimentary Research* 40, 695–707.
- Dickinson, W.R., 1985. Interpreting provenance relations from detrital modes of sandstones. In: Zuffa, G.G. (Ed.), *Provenance of Arenites North Atlantic Treaty Organization - Advanced Study Institutes (NATO-ASI)*, Series Cvol. 148, pp. 333–361.
- Dickinson, W.R., Suckcek, C.A., 1979. Plate-tectonics and sandstone compositions. *American Association Petroleum Geology Bulletin* 63 (12), 2164–2182.
- Dickinson, W.R., Beard, L.S., Brakenridge, G.R., Erjavec, J.L., Ferguson, R.C., Inman, K.F., Knepp, R.A., Lindberg, F.A., Ryberg, P.T., 1983. Provenance of North American Phanerozoic sandstones in relation to tectonic setting. *Geological Society of America Bulletin* 94, 222–235.
- Doglioni, C., 1992. Main differences between thrust belts. *Terra Nova* 4, 152–164.
- Doglioni, C., Mongelli, F., Pialli, G., 1998. Boudinage of the Alpine belt in the Apenninic back-arc. *Memoria della Società Geologica Italiana* 52, 457–468.
- Doglioni, C., Fernandez, M., Gueguen, E., Sabat, F., 1999. On the interference between the early Apennines-Maghrebides back-arc extension and the Alps-Betics orogen in the Neogene geodynamics of the Western Mediterranean. *Bollettino della Società Geologica Italiana* 118, 75–89.
- Drits, V.A., Sakharov, B.A., Lindgreen, H., Salyn, A., 1997. Sequential structure transformation of illite-smectite-vermiculite during diagenesis of Upper Jurassic shales from the North Sea and Denmark. *Clay Minerals* 32, 351–371.
- Dunham, R.J., 1962. Classification of carbonate rocks according to depositional texture. In: Ham, W.E. (Ed.), *Classification of Carbonate Rocks-A Symposium*. American Association Petroleum Geologists vol. 1, pp. 108–121.
- Durand-Delga, M., Rossi, M., Olivier, P., Puglisi, D., 2000. Situation structurelle et nature ophiolitique des roches basiques jurassiques associées aux flysch maghrébins du Rif (Maroc) et de Sicile (Italie). *C.R. de l'Académie des Sciences, Ser. IIA-Earth Planet Sciences* 331 pp. 29–38.
- El Mrihiet, A., Chaluan, A., Michard, A., 2004. Deformation style and kinematics of Mauretanian flysch-nappe: northwestern Rif Belt, Morocco. *32mo International Geological Congress, Abstract* 32, p. 770.
- El Ouahabi, M., Daoudi, L., Fagel, N., 2014. Mineralogical and geotechnical characterization of clays from northern Morocco for their potential use in the ceramic industry. *Clay Minerals* 49, 35–51.
- Eslinger, E., Mayer, L., Durst, T., Hower, J., Savin, S., 1973. A X-ray technique for distinguishing between detrital and secondary quartz in the fine grained fraction of sedimentary rocks. *Journal of Sedimentary Petrology* 43, 540–543.
- Faccenna, C., Becker, T.W., Lucente, F.P., Jolivet, L., Rossetti, F., 2001. History of subduction and back-arc extension in the Central Mediterranean. *Geophysical Journal International* 145, 809–820.
- Faleh, A., Sadiki, A., 2002. Glissement rotatif de Dhar El Harrag: exemplified'instabilité de terrain dans le Préf central (Maroc). *Bulletin de l'Institut Scientifique, Rabat* 24, 41–48.
- Finetti, I., 2005. CROP PROJECT: Deep Seismic Exploration of the Central Mediterranean and Italy. Elsevier Science Ltd., Amsterdam (ISBN: 9780080457604. 794 pp.).
- Folk, R.L., 1980. Petrology of Sedimentary Rocks. Hemphill's Austin (184 pp.).
- Garzanti, E., 2017. The maturity in sedimentology and provenance analysis. *Journal of Sedimentary Research* 87, 353–365.
- Gasparo Morticelli, M., Valenti, V., Catalano, R., Sulli, A., Agate, M., Avellone, G., Albanese, C., Basilone, L., Gugliotta, C., 2015. Deep controls on foreland basin system evolution along the Sicilian fold and thrust belt. *Bulletin de la Société Géologique de France* 186 (4–5), 273–290.
- Gazzi, P., 1966. Le arenarie del flysch soprarettaceo dell'Appennino modenese; correlazioni con il flysch di Monghidoro. *Mineralogica et Petrographica Acta* 12, 69–97.
- Giunta, G., Nigro, F., Renda, P., Giorgianni, A., 2000. The Sicilian-Maghrebides Tyrrenian margin: a neotectonic evolutionary model. *Bollettino della Società Geologica Italiana* 119, 553–565.
- Guerrera, F., Martín-Martín, M., 2014. Geodynamic events reconstructed in the Betic, Maghrebian, and Apennine chains (central-western Tethys). *Bulletin de la Société Géologique de France* 185, 329–341.
- Guerrera, F., Martín-Algarra, A., Perrone, V., 1993. Late Oligocene-Miocene syn-/late-orogenic successions in Western and Central Mediterranean Chains from the Betic Cordillera to the Southern Apennines. *Terra Nova* 5, 525–544.
- Guerrera, F., Martín-Martín, M., Perrone, V., Tramontana, M., 2005. Tectono-sedimentary evolution of the southern branch of the Western Tethys (Magrebian Flysch Basin and Lucanian Ocean). *Terra Nova* 17, 358–367.
- Guerrera, F., Antonio Estévez, A., López-Arcos, M., Martín-Martín, M., Martín-Pérez, J.A., Francisco Serrano, F., 2006. Paleogene tectono-sedimentary evolution of the Alicante Trough (External Betic Zone, SE Spain) and its bearing on the timing of the deformation of the South-Iberian Margin. *Geodinamica Acta* 19, 87–101.
- Guerrera, F., Mancheño, M.A., Martín-Martín, M., Raffaelli, G., Rodríguez-Estrella, Serrano, F., 2014. Paleogene evolution of the External Betic Zone and geodynamic implications. *Geodinamica Acta* 12, 171–192.
- Guerrera, F., Martín-Martín, M., Raffaelli, G., Tramontana, M., 2015. The Early Miocene "Bisciaro volcanoclastic event" (northern Apennines, Italy): a key study for the geodynamic evolution of the Central-Western Mediterranean. *International Journal of Earth Sciences (Geol Rundsch)* 104, 1083–1106.
- Guerrera, F., Martín-Martín, M., Tramontana, M., 2021. Evolutionary geological models of the central-western peri-Mediterranean chains: a review. *International Geology Review* 63, 65–86.
- Henriet, M., Dominguez, S., Barreca, G., Malavieille, J., Monaco, C., 2020. Structural and tectono-stratigraphic review of the Sicilian orogen and new insights from analogue modeling. *Earth-Science Reviews*, 103257. <https://doi.org/10.1016/j.earscirev.2020.103257>.
- Holtzapffel, T., 1985. Les minéraux argileux : préparation, analyse diffractométrique et détermination. *Société Géologique du Nord* 12 (136 pp.).
- Hunziker, J.C., 1986. The evolution of illite to muscovite: an example of the behavior of isotopes in low grade metamorphic terrains. *Chemical Geology* 57, 31–40.
- Ingersoll, R.V., Bullard, T.F., Ford, R.L., Grimm, J.P., Pickle, J.D., Sares, S.W., 1984. The effect of grain size on detrital modes: a test of the Gazzi-Dickinson point-counting method. *Journal of Sedimentary Research* 54, 103–116.
- Jabaloy-Sánchez, A., Azdimousa, A., Booth-Rea, G., Asebriy, L., Vázquez-Vilchez, M., Martínez-Martínez, J.M., Gabites, J., 2015. The structure of the Temsamane fold-and-thrust stack (eastern Rif, Morocco): evolution of a transpressional orogenic wedge. *Tectonophysics* 663, 150–176.
- Khomsi, S., Bédir, M., Soussi, M., Ben Jemia, M.G., Ben Ismail-Latrache, K., 2006. Highlight of middle-late Eocene compressional events in the subsurface of eastern Tunisia (Sahel): generality of the Atлас phase in North Africa. *Comptes Rendus Geoscience* 338, 41–49.
- Khomsi, S., Ben Jemia, M.G., Frizon de Lamotte, D., Maherssi, C., Echihhi, O., Mezni, R., 2009. An overview of the late cretaceous–Eocene positive inversions and oligo-Miocene subsidence events in the foreland of the Tunisian atlas: structural style and implications for the tectonic agenda of the Maghrebian atlas system. *Tectonophysics* 475, 38–582.
- Lanson, B., Sakharov, B.A., Claret, F., Drits, V.A., 2009. Diagenetic smectite-to-illite transition in clay-rich sediments: a reappraisal of X-ray diffraction results using the multi-specimen method. *American Journal of Science* 309, 476–516.
- Le Breton, E., Brune, S., Ustaszewski, K., Zahirovic, S., Seton, M., Müller, R.D., 2021. Kinematics and extent of the Piemont-Liguria Basin—implications for subduction processes in the Alps. *Solid Earth* 12, 885–913.
- Lentini, F., Carbone, S., 2014. *Geologia della Sicilia - Geology of Sicily. Memorie Descrittive della Carta Geologica D'Italia* 95 pp. 7–414.
- Leprêtre, R., Frizon de Lamotte, D., Combier, V., Gimeno-Vives, O., Mohn, G., Eschard, R., 2018. The Tell-Rif orogenic system (Morocco, Algeria, Tunisia) and the structural heritage of the southern Tethys margin. *Bulletin Société géologique France, Earth Sciences Bulletin* 189, 10.
- Lespinasse, P., 1977. Les marnes a block de la région de Zoumi. Evolution structural des zones externes du Rif (Maroc). *Bulletin de la Société Géologique de France* 19, 781–787.
- Lirer, F., Foresi, L.M., Iaccarino, S., Salvatorini, G., Turco, E., Cosentino, C., Sierra, F.J., Caruso, A., 2019. Mediterranean Neogene planktonic foraminifer biozonation and biochronology. *Earth-Science Reviews* 196, 102869. <https://doi.org/10.1016/j.earscirev.2019.05.013>.
- Lourens, L.J., Hilgen, F.J., Laskar, J., Shackleton, N.J., Wilson, D., 2004. The Neogene Period. In: Gradstein, F.M., Ogg, J.G., Smith, A.G. (Eds.), *A Geologic Time Scale 2004*. Cambridge University Press, pp. 409–440.
- Lustrino, M., Fedele, L., Melluso, L., Morra, V., Ronga, F., Geldmacher, J., Duggen, S., Agostini, S., Cucciniello, C., Franciosi, L., Meisel, T., 2013. Origin and evolution of Cenozoic magnetism of Sardinia (Italy). A combined isotopic (Sr-Nd-Pb-O-Hf-Os) and petrological view. *Lithos* 180–181, 138–158.
- Maaté, A., 1996. *Estratigrafía y evolución paleogeográfica del Dominio Gomáride (Rif Interno, Marruecos)*. (Tesis Doctoral)Universidad de Granada (397 pp.).
- Maaté, S., 2017. Evolution tectono-sédimentaire de la zone intrarifaine occidentale durant le Tertiaire (Marge africaine rifaine, Maroc). Corrélations avec la marge Tellienne tunisienne. Thèse Doctoral Université Abdelmalek Essâadi, Tétouan (Maroc) (206 pp.).
- Maaté, S., Alcalá, F.J., Guerrera, F., Hlila, R., Maaté, A., Martín-Martín, M., Raffaelli, G., Serrano, F., Tramontana, M., 2017. The External Tanger Unit (Intrarifsub-Domain, External Rifian zones, Morocco): an interdisciplinary study. *Arabian Journal of Geosciences* 10, 556. <https://doi.org/10.1007/s12517-017-3347-8>.
- Maaté, S., Guerrera, F., Hlila, R., Maaté, A., Martín-Martín, M., Tramontana, M., 2018. New structural data on Tertiary of the External Tanger Unit (Intrarif, Morocco). *Geogaceta* 63, 123–126.
- Martín-Algarra, A., 1987. Evolución geológica Alpina del contacto entre las Zonas Internas y las Zonas Externas de la Cordillera Bética. (Unpublished PhD Thesis) Universidad de Granada (1171 pp.).
- Martín-Martín, M., Rey, J., Alcalá, F.J., Tosquella, J., Deramond, J., Lara-Corrona, E., Duranthon, F., Antoine, P.O., 2001. Tectonic controls on the deposits of a foreland basin: an example from the Eocene Corbières-Minervois basin, France. *Basin Research* 13, 419–433.
- Martín-Martín, M., Guerrera, F., Alcalá, F.J., Serrano, F., Tramontana, M., 2018. Source areas evolution in the Neogene Agost Basin (Betic Cordillera): implications for regional reconstructions. *Italian Journal of Geosciences* 137, 433–451.
- Martín-Martín, M., Guerrera, F., Hlila, R., Maaté, S., Tramontana, M., Serrano, F., Cañaverales, J.C., Alcalá, F.J., Paton, D., 2022a. Tectono-sedimentary Cenozoic evolution of the El Habt and Ouezzane Tectonic units (External Rif, Morocco). *Geosciences* 18, 850–884.
- Martín-Martín, M., Guerrera, F., Maaté, A., Hlila, R., Serrano, F., Cañaverales, J.C., Paton, D., Alcalá, F.J., Maaté, S., Tramontana, M., Martín-Pérez, J.A., 2022b. The Cenozoic evolution of the Intrarif (Rif, Morocco). *Geosphere* 18 (2), 850–884.
- Martín-Martín, M., Guerrera, F., Cañaverales, J.C., Alcalá, F.J., Serrano, F., Maaté, A., Hlila, R., Maaté, S., Tramontana, M., Sánchez-Navas, A., Le Breton, E., 2023. Paleogene evolution of the African Plate northwestern margin (External Rif Zone, Morocco) and comparison with other western Tethyan margins. *Sedimentary Geology* 448, 106367. <https://doi.org/10.1016/j.sedgeo.2023.106367>.
- Martín-Ramos, J.D., Díaz-Hernández, J.L., Cambeses, A., Scarrow, J.H., López-Galindo, A., 2012. Pathways for quantitative analysis by X-ray diffraction. In: Aydinalp, C. (Ed.),

- An Introduction to the Study of Mineralogy. Tech, Rijeka, Croatia, CumhurAydinalp. Intech Open, pp. 73–92.
- Miall, A., 2016. The valuation of unconformities. *Earth-Science Reviews* 163, 22–71.
- Michard, A., Chalouan, A., Feinberg, H., Goffé, B., Montigny, R., 2002. How does the Alpine belt end at Gibraltar ? A collage astride a plate boundary in the West Mediterranean area (Morocco, Spain). *Bulletin de la Société Géologique de France* 173, 3–15.
- Michard, A., Frizon de Lamotte, D., Liégeois, J.-P., Saddiqi, O., Chalouan, A., 2008. Conclusion: continental evolution in western Maghreb. In: Michard, A., Saddiqi, O., Chalouan, A., Frizon de Lamotte, D. (Eds.), *Lecture Notes in Earth Sciences*. 116 (404 pp.).
- Michard, A., Mokhtari, A., Chalouan, A., Saddiqi, O., Rossi, Ph., Rjimati, E.-C., 2014. New ophiolite slivers in the External Rif belt, and tentative restoration of a dual Tethyan suture in the western Maghrebides. *Bulletin de la Société Géologique de France* 185, 313–328.
- Michard, A., Mokhtari, A., Lach, Ph., Rossi, Ph., Chaouan, A., Saddiqi, O., Rjimati, E.-C., 2018. Liassic age of an oceanic gabbro of the External Rif (Morocco): implications for the Jurassic continent-ocean boundary of Northwest Africa. *Comptes Rendus Geoscience* 350, 299–309.
- Moiroud, A., Martinez, M., Deconinck, J.F., Monna, F., Pellenard, P., Riquier, L., Company, M., 2012. High-resolution clay mineralogy as a proxy for orbital tuning: example of the Hauterivian-Barremian transition in the Betic Cordillera (SE Spain). *Sedimentary Geology* 282, 336–346.
- Moore, D.M., Reynolds, R.C., 1997. *X-ray Diffraction and the Identification and Analysis of Clay Minerals*. 2nd ed. Oxford University Press, Oxford, New York (378 pp.).
- Müller, R.D., Zhirovic, S., Williams, S.E., Cannon, J., Seton, M., Bower, D.J., Tetley, M.G., Heine, C., Le Breton, E., Liu, S., 2018. A Global Plate Model including lithospheric deformation along major rifts and orogens since the Triassic. *Tectonics* 38, 1884–1907.
- Müller, R.D., Zahirovic, S., Williams, S.E., Cannon, J., Seton, M., Bower, D.J., Tetley, M.G., Heine, C., Le Breton, E., Liu, S., Russel, S.H.J., Yang, T., Leonard, J., Gurnis, M., 2019. A global plate model including lithospheric deformation along major rifts and orogens since the Triassic. *Tectonics* 38, 1884–1907.
- Nieto, E., Ortega-Huertas, M., Peacor, D.R., Aróstegui, J., 1996. Evolution of illite/smectite from early diagenesis through incipient metamorphism in sediments of the Basque-Cantabrian basin. *Clays and Clay Minerals* 44, 304–323.
- Novak, A., Egenhoff, S., 2019. Soft-sediment deformation structures as a tool to recognize synsedimentary tectonic activity in the middle member of the Bakken Formation, Williston Basin, North Dakota. *Marine and Petroleum Geology* 105, 124–140. <https://doi.org/10.1016/j.marpetgeo.2019.04.012>.
- Pletsch, T., 1997. Clay minerals in Cretaceous deep-water formations of the Rif and the Betic Cordillera. *Bulletin de la Société Géologique du Nord* 26, 1–106.
- Pletsch, T., Daoudi, L., Chamley, H., Deconinck, J.F., Charroud, M., 1996. Palaeogeographic controls on palygorskite occurrence in mid-Cretaceous sediments of Morocco and adjacent basins. *Clay Minerals* 31, 403–416.
- Righi, D., Elsass, F., 1996. Characterization of soil clay minerals: decomposition of X-ray diffraction diagrams and high-resolution electron microscopy. *Clays and Clay Minerals* 44, 791–800.
- Rossetti, F., Dini, A., Lucci, F., Bouybaouenne, M., Faccenna, C., 2013. Early Miocene strike-slip tectonics and granite emplacement in the Alboran Domain (Rif Chain, Morocco): significance for the geodynamic evolution of Western Mediterranean. *Tectonophysics* 608, 774–791.
- Rouvier, H., 1977. *Géologie de l'extrême Nord Tunisien: tectoniques et paléogéographies superposées à l'extrémité orientale de la chaîne Nord Maghrébine. VI*. Thèse Science Université Paris (703 pp.).
- Rouvier, H., 1985. *Géologie de l'Extrême Nord Tunisien: tectonique et paléogéographie superposées à l'extrémité orientale de la chaîne nord- maghrébine*. Edition du Service géologique de Tunisie. Annales des mines et de la géologie p. 29 (427 pp.).
- Royden, L.H., 1993. Evolution of retreating subduction boundaries formed during continental collision. *Tectonics* 12, 626–638.
- Schettino, A., Turco, E., 2011. Tectonic history of the western Tethys since the Late Triassic. *Geological Society of America Bulletin* 123, 89–105.
- Schultz, L.G., 1964. Quantitative Interpretation of Mineralogical Composition From X-ray and Chemical Data for the Pierre Shale. U.S. Geological Survey, Professional Paper 391-C (31 pp.).
- Serrano, F., 1992. Biostratigraphic control of Neogene volcanism in Sierra de Gata (South-east Spain). *Geologie en Mijnbouw* 71, 3–14.
- Stampfli, G.M., Borel, G.D., Marchant, R., Mosar, J., 2002. Western Alps geological constraints on western Tethyan reconstructions. In: Rosenbaum, G., Lister, G.S. (Eds.), *Reconstruction of the Evolution of the Alpine-Himalayan orogen*. Journal Virtual Explorer, pp. 77–106.
- Stampfli, G.M., Kozur, 2006. Europe from the Variscan to the Alpine Cycles. *Geological Society of London* 32, 5782.
- Suter, G., 1980a. *Carte Géologique du Rif*, 1/500000. Notes et Mémoires du Service Géologique du Maroc p. 245a.
- Suter, G., 1980b. *Carte Structurale de la Chaînerifaine à 1/500000*. Notes et Mémoires du Service Géologique du Maroc p. 245b.
- Tejera de Leon, J., Duée, G., 2003. Relationships Between the Neogene Foredeep Basins of the Western External Rifian Belt Related to the Arbaoua-Jebha Transform Fault. Consequences for the Interpretation of the Evolution of the Rifian belt (Morocco). *Travaux Institute Scientifique Rabat (Rabat, Morocco), série Géologie & Géographie Physique* 21 pp. 1–19.
- Tek, D.E., Poyatos-Moré, M., Patacci, M., McArthur, A.D., Colombera, L., Cullen, T.M., McCaffrey, W.D., 2020. Syndepositional tectonics and mass-transport deposits control channelized, bathymetrically complex deepwater systems (Aïnsa depocenter, Spain). *Journal of Sedimentary Research* 90 (7), 729–762 ISSN 1527-1404 <https://doi.org/10.2110/jsr.2020.38>.
- Tortosa, A., Palomares, M., Arribas, J., 1991. Quartz grain types in Holocene deposits from the Spanish Central System: some problems in provenance analysis. In: Morton, A.C., Todd, S.P., Haughton, P.D.W. (Eds.), *Developments in Sedimentary Provenance Studies*. Geological Society of London, Special Publications vol. 57, pp. 47–54.
- Van Houten, F.B., 1980. Mid-Cenozoic Fortuna Formation, northeastern Tunisia—record of late Alpine activity on North African Cratonic Margin. *American Journal of Science* 280, 1051–1062.
- Vázquez, M., Asebriy, L., Azdimousa, A., Jabaloy, A., Booth-Rea, G., Barbero, L., Mellini, M., González-Lodeiro, F., 2013. Evidence of extensional metamorphism associated to Cretaceous rifting of the North-Maghrebian passive margin: the Tanger-Ketama unit (external Rif, northern Morocco). *Geologica Acta* 11, 277–293.
- Vera, J.A., 2000. El Terciario de la Cordillera Bética: estado actual de conocimientos. *Revista de la Sociedad Geológica de España* 12, 345–373.
- Vera, J.A., 2004. *Geología de España. Sociedad Geológica de España; Instituto Geológico y Minero de España* (884 pp.).
- Vitali, S., Amore, O.F., Ciarcia, S., Fedele, L., Griffa, C., Prinzi, E.P., Tavani, S., Tramparulo, F.D., 2017. Structural, stratigraphic, and petrological clues for a Cretaceous–Paleogene abortive rift in the southern Adria domain (southern Apennines, Italy). *Geological Journal* <https://doi.org/10.1002/gj.2919>.
- Wildi, W., 1983. La charne tello-rifaine (Algérie, Maroc, Tunisie): structure, stratigraphie et évolution du Trias au Miocène. *Revue de Géographie Physique et de Géologie Dynamique* 24, 201–297.
- Zaghoul, M.N., Di Staso, A., Gigliuto, L.G., Maniscalco, R., Puglisi, D., 2005. Stratigraphy and provenance of Lower and Middle Miocene strata within the External Tanger Unit (Intra-Rif sub-Domain, External Domain; Rif, Morocco): first evidence. *Geologica Carpathica* 56, 517–530.
- Zakir, A., Chalouan, A., Feinberg, H., 2004. Evolution tectono-sédimentaire d'un domaine d'avant-chaîne: exemple des basins d'El-Habit et de Sidi Mrayt, Rif externe nord-occidental (Maroc); précisions stratigraphiques et modélisation tectonique. *Bulletin de la Société Géologique de France* 175, 383–397.
- Zuffa, G.G., 1980. Hybrid arenites: their composition and classification. *Journal of Sedimentary Petrology* 50, 21–29.
- Zuffa, G.G., 1985. Optical analyses of arenites: Influence of methodology on compositional results. In: Zuffa, G.G. (Ed.), *Provenance of Arenites NATO ASI Series (Series C: Mathematical and Physical Sciences)* vol. 148. Springer, Dordrecht, pp. 165–189.
- Zuffa, G.G., 1987. Unravelling hinterland and offshore palaeogeography from deep-water arenites. In: Leggett, J.K., Zuffa, G.G. (Eds.), *Marine Clastic Sedimentology: Concepts and Case Studies*. Graham and Trotman, London, pp. 39–61.